

Accuracy of experimentally estimated muscle properties: Evaluation and improvement using a newly developed toolbox

Edwin D.H.M. Reuvers¹,  and Dinant A. Kistemaker¹ 

¹ Department of Human Movement Sciences, Faculty of Behavioural and Movement Sciences, Vrije Universiteit Amsterdam, Amsterdam Movement Sciences, The Netherlands

 Corresponding author: Edwin D.H.M. Reuvers (edwin.reuvers.academia@pm.me)

Access the code and full analysis notebook at <https://edwinreuvers.github.io/publications/acc-mp-estimation/>

Abstract

The mechanical behaviour of a muscle-tendon complex depends on properties such as the force-length relationships, the force-velocity relationship, and the excitation dynamics. Quick-release and step-ramp experiments are commonly used to estimate these properties. The accuracy of these methods is unclear, as the actual values of these properties are unknown in experiments on real muscle. We conducted a modelling study using a Hill-type muscle-tendon complex model with literature-derived parameter values and simulated quick-release, step-ramp, and isometric experiments. From the simulated experiments, we assessed how accurately the model's parameter values could be retrieved. Using a method traditionally used in literature, the series elastic element stiffness was underestimated by ~35%, due to the incorrect assumption that muscle fibres do not shorten during quick releases. Consequently, this yielded an overestimation of the excitation dynamics activation time constants of ~20%. We developed an improved method that accounted for muscle fibre length shortening during quick releases. Using our improved method, all parameter values closely matched their actual values. A sensitivity analysis showed that the most critical parameters were robust to perturbations in experimental data. Lastly, we compared Hill-type MTC model predictions against *in situ* data from three rat m. gastrocnemius medialis muscles. Predictions based on parameters from the improved method showed closer agreement than those based on the traditional method — both for quick-release, step-ramp, and isometric experiments, as well as for independent stretch-shortening cycles. In conclusion, the improved method enables more accurate estimates of muscle-tendon complex properties, addressing limitations of the traditionally used method.

1 Introduction

2 In the early 20th century, A.V. Hill laid the foundation of muscle mechanics by recognising that muscles
3 contain not only muscle fibres (the contractile element; CE) but also connective tissue, both parallel
4 to the muscle fibre (the parallel elastic element; PEE) and in series with the muscle fibre (the tendon
5 or serial elastic element; SEE). Together these three elements form the muscle-tendon-complex (MTC).
6 The contraction dynamics describe how CE force emerges from the interplay between the force-length
7 properties of CE, PEE and SEE, and the force-velocity properties of CE. In addition, CE force depends on
8 the active state (the relative amount of Ca^{2+} bound to troponin C, [Ebashi and Endo, 1968](#)). Active state, in
9 turn, depends on activation via the excitation dynamics. Consequently, the mechanical behaviour of MTC
10 arises from the intricate interplay between the contraction and the excitation dynamics.

11 In his famous ([1938](#)) paper A.V. Hill performed so-called ‘isotonic quick-release experiments’ using the
12 now-renowned Levin-Wyman lever ([Levin and Wyman, 1927](#)) to estimate the CE force-velocity relationship.
13 In these experiments, MTC was attached to a lever and maximally stimulated. When SEE force plateaued
14 (i.e., MTC was isometrically delivering force), a magnet was released from the lever causing a sudden drop
15 in the force acting on the MTC. As SEE force remained constant right after this drop in SEE force, SEE
16 length remained constant and therefore all MTC length changes were attributed to CE length changes. The
17 CE velocity corresponding to the constant SEE force after the drop was then calculated as the maximum
18 rate of change of MTC length over time. Consequently, each isotonic quick-release experiment contributed
19 a single data point of the CE force-velocity relationship. Nowadays, servomotors are typically used in
20 experiments on isolated MTCs to control MTC length (changes). In contrast to the force-controlled
21 experiments with the Levin-Wyman lever, servomotor control the MTC length over time (see Figure [S1](#)).
22 In order to estimate the CE force-velocity relationship using a servomotor, Cecchi et al. ([1978](#)) introduced
23 ‘step-ramp experiments’. In these experiments, MTC is kept isometrically under maximal stimulation
24 until SEE force plateaus. Then, a rapid shortening of MTC length is imposed (the ‘step’), immediately
25 followed by a constant-velocity shortening of the MTC (the ‘ramp’). This experimental protocol results
26 in a brief plateau in SEE force just after the ramp. During this brief period, SEE length remains constant
27 and therefore CE velocity equals MTC velocity. Thus, step-ramp experiments with servomotors serve as a
28 valid alternative for isotonic quick-release experiments to estimate the CE force-velocity relationship.

29 In addition to estimating the CE force-velocity relationship using isotonic quick-release experiments, the
30 research group of A.V. Hill also used these experiments to approximate SEE stiffness. The underlying
31 idea was that the drop in MTC force was so fast that, due to contraction dynamics, CE had no time to
32 shorten and all MTC shortening could thus be directly attributed to SEE shortening. Consequently, this
33 experiment allowed to directly relate SEE length changes to changes in SEE force and therefore to estimate
34 SEE stiffness. As mentioned above, in isotonic quick-release experiments, a sudden drop in force acting
35 on the MTC causes a rapid change in MTC length. While in these lever-based experiments MTC force is
36 controlled, in experiments using a servomotor MTC length is controlled. To estimate SEE stiffness with a
37 servomotor setup, the opposite approach is taken: a rapid change in MTC length is imposed by the motor,
38 resulting in a rapid change in SEE force. Somewhat confusingly, these servomotor-based experiments are

also referred to as ‘quick-release experiments’, even though their approach differs fundamentally from that of an isotonic quick-release experiment. In the remainder of this paper, the term quick-release experiments will exclusively refer to servomotor-based length-controlled quick-release experiments. In quick-release experiments using a servomotor, the drop in MTC length takes several milliseconds (e.g., approximately 10 ms with the commonly used Aurora Scientific’s 300C series motor). As CE shortens within this short time period, the assumption that MTC length changes are exclusively due to SEE length changes may not be entirely valid. This raises the question to what extent SEE stiffness can be accurately estimated based on quick-release experiments using servomotors.

A.V. Hill already acknowledged in (1950) that CE shortens during the brief period in which SEE force decreases – even for his isotonic quick-release experiments using the Levin-Wyman lever – and introduced a method to correct for this CE shortening. In this method, the CE shortening that occurred due to the quick-release was estimated based on the CE force-velocity relationship of the MTC investigated. Thus, additional experimental work – such as performing step-ramp experiments and estimating the CE force-velocity relationship – are required to correct for CE shortening during the quick-release. Zandwijk et al. (1997) and Lemaire et al. (2016) developed similar methods to correct for CE shortening. As expected, Zandwijk et al. (1997) showed that this method results in higher estimates of SEE stiffness than with the method without correcting for CE shortening. Nevertheless, the accuracy of SEE stiffness estimates remains uncertain, as the actual SEE stiffness is unknown in experiments, making it infeasible to compare the estimated value against the actual one. Consequently, it remains unclear whether the additional complexity and experimental work required for the improved method are truly justified in comparison with the simpler traditional method, especially when the only interest is SEE stiffness.

In experimental studies in which MTC properties are estimated, SEE stiffness is typically estimated first in order to discriminate between SEE stiffness and the other properties, such as those of the CE force-length relationship. In experiments, CE length is unknown and therefore the properties of the CE force-length relationship cannot be directly estimated based on experimental data. Typically, the CE force-length properties are estimated based on the measured MTC force-length relationship (e.g., Blümel et al., 2012; Lemaire et al., 2016). However, different combinations of CE and SEE properties can yield almost identical MTC force-length relationships. Consequently, inaccuracies in SEE stiffness estimates can propagate to errors in the estimation of the CE force-length properties. While predictions under isometric conditions may remain reasonably accurate, these errors can lead to substantially different mechanical behaviour during dynamic contractions such as stretch-shortening cycles (see Figure 1). As such, incorrect estimation of SEE stiffness might (partially) explain difference between predictions derived by a Hill-type MTC model and experimental results. In sum, the question arises to which extent the estimates of other MTC properties are affected by inaccurate SEE stiffness estimates and whether more accurate SEE stiffness estimates improves predictions derived by a Hill-type MTC model.

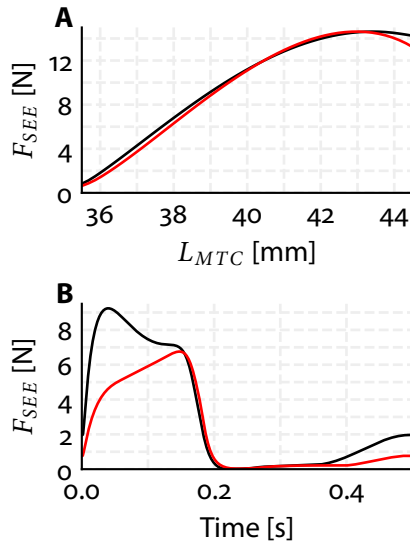


Figure 1: Effect of a 2.5-fold difference in SEE stiffness on simulated mechanical behaviour. This example shows that some contractions may lead to similar mechanical behaviour across distinct parameter sets, others may differ substantially.

74 The potential effect of error propagation also extends to the estimation of the excitation dynamics properties.
 75 In the absence of histochemical data, excitation dynamics properties are commonly estimated by fitting
 76 predicted SEE force of the Hill-type MTC model to experimental data (e.g., Blümel et al., 2012; Lemaire
 77 et al., 2016). As SEE force over time obviously depend on the contraction dynamics properties (e.g., the
 78 force-length relationships and the force-velocity relationship), the estimation of the excitation dynamics
 79 properties is not independent of the estimation of the contraction dynamics properties. Consequently,
 80 inaccuracies in SEE stiffness estimates can propagate to inaccuracies in estimated excitation dynamics
 81 properties. This interdependence raises an additional question of what experimental data should be used
 82 in order to minimise this potential error propagation.

83 The primary objective of this study was to systematically evaluate the accuracy of estimating contraction and
 84 excitation dynamics properties on the basis of data collected in commonly used experiments. Specifically,
 85 we aimed to compare the results of a method that does not correct for CE shortening in quick-release
 86 experiments (the ‘traditional method’) with a method that does correct for CE shortening (the ‘improved
 87 method’). As explained earlier, the limitation of relying exclusively on an experimental approach is that
 88 the actual properties are unknown, which renders a reliable assessment of the accuracy of the estimated
 89 properties not feasible. To circumvent this problem, we conducted a modelling study using a Hill-type
 90 MTC model. First, we obtained three different sets of parameter values of a Hill-type MTC model from
 91 existing literature. Using these parameter values, we simulated data of quick-release, step-ramp and
 92 isometric protocols mimicking experiments on isolated MTCs using servomotors. We then investigated
 93 how accurately we could retrieve the model’s parameter values (with respect to their ‘actual’ value). In
 94 addition, we employed a comprehensive sensitivity analysis to assess the sensitivity of parameter values
 95 against perturbations in experimental data and to examine the interdependency of the estimated properties.
 96 The secondary objective of this study was to evaluate whether predictions from a Hill-type MTC model

97 using parameter values estimated with the improved method better matched experimental data than
98 predictions using parameter values estimated with the traditional method. To this end, we used *in situ* data
99 from experiments on three rat m. gastrocnemius medialis. We estimated the contraction and excitation
100 dynamics properties using both the traditional and the improved method, and compared the resulting
101 model predictions — based on each parameter set — to experimental force data. Overall, this study provides
102 insights into the accuracy of existing commonly used methods for contraction and excitation dynamics
103 property estimation and their influence on predictions of mechanical behaviour derived by a Hill-type MTC
104 model. The approach that we designed in this study for estimating contraction and excitation dynamics
105 properties based on data of quick-release, step-ramp and isometric experiments using servomotors, is
106 made available as an open-source toolbox (<https://github.com/edwinreuvers/mp-estimator>).

107 **2 Methods**

108 The primary objective of this study was to assess the accuracy of estimating contraction and excitation
109 dynamics properties. For this purpose, we employed a Hill-type MTC model to simulate MTC mechanical
110 behaviour, as detailed in Section 2.1. Using parameter values obtained from existing literature, we simulated
111 data of quick-release, step-ramp, and isometric experiments, mimicking experiments on isolated MTCs
112 with servomotors, as described in Section 2.2.1. We then estimated the contraction and excitation dynamics
113 parameter values using two methods: one with (the ‘traditional method’) and one without (the ‘improved
114 method’) a correction for CE shortening due to the quick-release (see Section 2.3). Additionally, we
115 conducted comprehensive sensitivity analyses to assess the accuracy of the improved method, as outlined
116 in Section 2.4. The secondary objective was to evaluate predictions derived by a Hill-type MTC model
117 using two sets of parameter values: one estimated by the traditional method, the other by the improved
118 method. For this purpose, we used *in situ* data (see Section 2.2.2) from three rat m. gastrocnemius
119 medialis. Predictions were assessed against quick-release, step-ramp, and isometric experiments, as well
120 as independently measured stretch-shortening cycles. This allowed us to investigate whether the improved
121 method enhanced the predictions derived by a Hill-type MTC model.

122 **2.1 Muscle model**

123 **2.1.1 Contraction dynamics**

124 We employed a Hill-type MTC model consisting of a contractile element (CE) and a parallel elastic element
125 (PEE), which were both in series with a serial elastic element (SEE), as depicted in Figure 2. CE represented
126 the contractile element of the muscle fibres, while PEE and SEE represented the tissues arranged in parallel
127 and in series with the muscle fibres, respectively. Given the negligible small mass of MTC compared to the
128 forces typically delivered by CE, PEE, and SEE, we simplified the model by neglecting the second-order
129 dynamics of the system:

$$\begin{aligned} L_{MTC} &= L_{CE} + L_{SEE} + \\ F_{SEE} &= F_{CE} + F_{PEE} \end{aligned} \tag{1}$$

130 L_{MTC} , L_{CE} , L_{SEE} and L_{PEE} denote MTC, CE, PEE and SEE length respectively, while F_{SEE} , F_{CE} , and F_{PEE}

¹³¹ denote the CE, PEE and SEE force. PEE and SEE were assumed be purely elastic and were modelled as
¹³² quadratic springs ([Zajac, 1989](#)):

$$F_{EE} = \begin{cases} k_{SEE} \cdot (l_{EE} - L_{EE}^o)^2, & \text{if } l_{EE} \geq L_{EE}^o \\ 0, & \text{otherwise} \end{cases} \quad (2)$$

¹³³ L_{EE} denotes the length of either PEE or SEE and L_{EE}^o the slack length of either PEE or SEE. k_{EE} denotes a
¹³⁴ parameter that scales the stiffness of either PEE or SEE.

¹³⁵ Isometric CE force depends on CE length ([Blix, 1892](#); [Blix, 1893](#); [Hill, 1925](#)). We simplified the classic
¹³⁶ sarcomere force-length relationship ([Gordon et al., 1966](#); [Walker and Schrodt, 1974](#)) to a second order
¹³⁷ polynomial, which describes the force-length relationship reasonably well ([Bobbert et al., 1990](#); [Woittiez et](#)
¹³⁸ [al., 1984](#)):

$$F_{CE}^{isom,rel} = \begin{cases} \frac{-1}{w^2} \cdot (L_{CE}^{rel} - 1)^2 + 1, & \text{if } F_{CE}^{isom,rel} > 0.1 \\ s_{exp} \cdot e^{k_{exp} \cdot L_{CE}^{rel}}, & \text{otherwise} \end{cases} \quad (3)$$

¹³⁹ $F_{CE}^{isom,rel}$ denotes the CE isometric force normalised by F_{CE}^{max} , w determines the width of the CE force-length
¹⁴⁰ relationship (for $F_{CE}^{isom,rel} > 0.1$) and L_{CE}^{rel} denotes CE length normalised by CE optimum length (L_{CE}^{opt} , the
¹⁴¹ CE length at $F_{CE}^{isom,rel} = 1$). Exponential tails were added to the isometric CE force-length relationship
¹⁴² such that it had a continuous first derivative with respect to L_{CE}^{rel} (see Figure 2). The parameter values of
¹⁴³ s_{exp} and k_{exp} were determined separately for the ascending and descending limb of the CE force-length
¹⁴⁴ relationship.

¹⁴⁵ The concentric CE force-velocity was modelled according to Hill ([1938](#)). The original description was
¹⁴⁶ adjusted as suggested by Soest and Bobbert ([1993](#)) to account for situations where the active state (q , the
¹⁴⁷ relative amount of Ca^{2+} bound to troponin C, [Ebashi and Endo, 1968](#)) is not maximal:

$$F_{CE} = \frac{q \cdot (F_{CE}^{isom,rel} \cdot F_{CE}^{max} \cdot b + a \cdot v_{CE})}{b - v_{CE}} \quad (4)$$

¹⁴⁸ F_{CE} denotes the CE force and v_{CE} denotes the CE velocity. a is a parameter that defines the curvature
¹⁴⁹ of the concentric CE force-velocity relationship and defines together with b and F_{CE}^{max} the maximum
¹⁵⁰ shortening velocity (v_{CE}^{max} , $v_{CE}^{max} = -b/a \cdot F_{CE}^{max}$). The maximum shortening velocity is scaled by $F_{CE}^{isom,rel}$
¹⁵¹ due to the formulation of the CE force-velocity relationship (see Equation 4). However, the maximum
¹⁵² shortening velocity has been reported to be more or less constant above optimum CE length ([Gordon et al.,](#)
¹⁵³ [1966](#); [Stern, 1974](#)). Based on this observation, the parameter a was scaled by $F_{CE}^{isom,rel}$ above optimum CE
¹⁵⁴ length ($L_{CE}^{rel} > 1$) to make the maximum shortening velocity independent of CE length above optimum CE
¹⁵⁵ length. The parameter b was scaled with b_{scale} for low levels of active state in order to make the maximal
¹⁵⁶ contraction velocity dependent on the active state ([Petrofsky and Phillips, 1981](#)). The original description
¹⁵⁷ of this scaling by Soest and Bobbert ([1993](#)) was somewhat reformulated, such that b_{scale} was continuously
¹⁵⁸ differentiable with respect to q :

$$b_{scale} = \frac{1}{1 + e^{-b_{shape} \cdot (q - q_{sc})}}$$

with $q_{sc} = \frac{\log(\frac{1}{b_{scale}^{min} - 1} + q_0 \cdot b_{shape})}{b_{shape}}$

(5)

¹⁵⁹ q_0 denotes the minimum value of q , b_{scale}^{min} denotes the minimal scale factor of b (i.e., the minimal value
¹⁶⁰ of b_{scale}) and b_{shape} defines the steepness of the relation between b_{scale} and q . The value of b_{shape} was
¹⁶¹ obtained by minimising the least square error between the formulation of Soest and Bobbert (1993) and
¹⁶² the reformulated version of the relation between b_{scale} and q .

¹⁶³ The eccentric part of the CE force-velocity relationship was modelled as a slanted hyperbola function
¹⁶⁴ (Soest et al., 2005) of the following form:

$$F_{CE}^{rel} = \frac{c_4 - (c_3 + v_{CE}^{rel} \cdot (c_1 + c_2 \cdot v_{CE}^{rel}))}{c_3 \cdot v_{CE}^{rel}}$$
(6)

¹⁶⁵ c_1 , c_2 , c_3 and c_4 denote parameters that define the shape of the slanted hyperbola and depend on $F_{CE}^{isom,rel}$
¹⁶⁶ and q . These parameters were chosen such that (1) the concentric and eccentric curves were continuous
¹⁶⁷ in the point $v_{CE}^{rel} = 0$; (2) the ratio between the eccentric and concentric derivatives of $\frac{dF_{CE}^{rel}}{dv_{CE}^{rel}}$ in the point
¹⁶⁸ $v_{CE}^{rel} = 0$ was defined by r_{slope} ; (3) the oblique asymptote of the eccentric curve was defined by F_{asympt} and
¹⁶⁹ (4) the slope of the slanted asymptote was defined by r_{as} .

¹⁷⁰ 2.1.2 Excitation dynamics

¹⁷¹ The excitation dynamics were modelled in two steps. The first step, to which we refer as the calcium
¹⁷² dynamics, related the rate of change in normalised free Ca^{2+} concentration between the myofilaments
¹⁷³ (γ) to normalised CE stimulation (*STIM*) and the normalised free Ca^{2+} concentration between the
¹⁷⁴ myofilaments itself (Hatze, 1981, pp 31-42):

$$\dot{\gamma} = \begin{cases} \frac{STIM \cdot (1 - \gamma_0) - \gamma + \gamma_0}{\tau_{act}}, & \text{if } STIM \geq \gamma \\ \frac{STIM \cdot (1 - \gamma_0) - \gamma + \gamma_0}{\tau_{deact}}, & \text{otherwise} \end{cases}$$
(7)

¹⁷⁵ γ_0 denotes the minimum value of γ and had an arbitrary small value such that Equation 8 was always
¹⁷⁶ solvable. τ_{act} and τ_{deact} are both time constants of the first-order differential equations describing the
¹⁷⁷ calcium dynamics. The second step involved the relation between active state (q) and γ , to which we refer
¹⁷⁸ as the $q - [Ca^{2+}]$ relation. It is well-known that muscle fibres become increasingly sensitive to $[Ca^{2+}]$ as
¹⁷⁹ their length increases (Kistemaker et al., 2005; Rack and Westbury, 1969; Stephenson and Williams, 1982).
¹⁸⁰ Consequently, q was also made dependent on L_{CE}^{rel} . The $q - [Ca^{2+}]$ relation was modelled according to
¹⁸¹ Hatze (1981, pp 31-42), but was mathematically reformulated to ensure that the parameter values were
¹⁸² physiologically meaningful and to facilitate its application for Optimal Control (e.g., Kistemaker et al.,
¹⁸³ 2023):

$$q = q_0 + \frac{1 - q_0}{1 + (kCa \cdot \gamma)^{A_{act}} \cdot e^{a_{act} \cdot B_{act}}} \quad (8)$$

with $A_{act} = \log_{10}(e^{-a_{act}})$
 and $B_{act} = b_{act,1} + b_{act,2} \cdot L_{CE}^{rel} + b_{act,3} \cdot L_{CE}^{rel^2}$

¹⁸⁴ kCa relates γ to the actual Ca^{2+} concentration between the myofilaments and B_{act} denotes the pCa^{2+}
¹⁸⁵ level at which $q = 0.5$. B_{act} depended on L_{CE}^{rel} (Equation 8), while parameter a_{act} determined the steepness
¹⁸⁶ of the relation between γ and q .

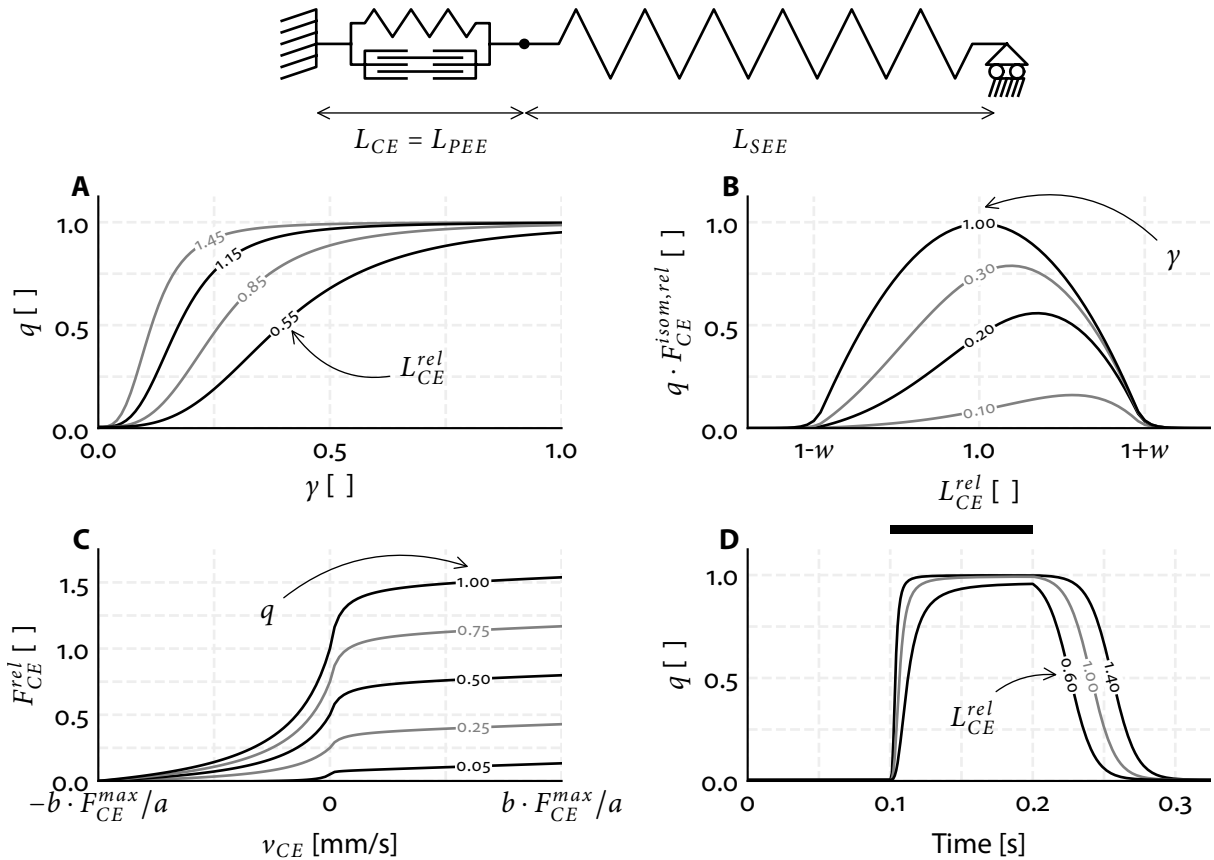


Figure 2: Aspects of the Hill-type MTC model used, illustrated at the top. L_{CE} , L_{PEE} and L_{SEE} denote the CE, parallel elastic element (SEE) and serial elastic element (SEE) length. CE represents the contractile part of the muscle fibres, while PEE and SEE represent all elastic tissue in parallel or in series, respectively, with CE. In the Hill-type MTC model, CE force depends on active state (q), CE length (B) and CE velocity (C). The effect of CE stimulation on active state (q) is illustrated in D. A) The relationship between normalized free Ca^{2+} concentration between the myofilaments (γ) and q . q also depends on relative CE length (L_{CE}^{rel}). B) The product of q and the normalized active CE force-length relationship for different values of γ . C) The CE force-velocity relationship for different values of q . D) q over time before, during and after CE stimulation for $L_{CE}^{rel} = 1$. CE stimulation is maximal during the period indicated by the black bar and ‘off’ elsewhere.

187 **2.2 Simulated and *in situ* data**

188 **2.2.1 Simulated data**

189 To simulate quick-release, step-ramp, and isometric experiments, we used three parameter sets of a Hill-
190 type MTC model from existing literature for three rat m. gastrocnemius medialis (GM1, GM2, and GM3;
191 see Table S1).

192 **Quick-release experiments** Each quick-release experiment consisted of an isometric phase until SEE
193 force plateaued, followed by a rapid (step) change (10 ms) in MTC length and then followed by another
194 isometric phase (see Figure 3A). CE stimulation was maximal (i.e., STIM = 1) during the first isometric
195 phase and continued at this maximal level until it was switched off shortly after the step change in MTC
196 length occurred. The step change in MTC length was 0.2 mm and was chosen such that the resulting
197 change in SEE force was about 5–10% of F_{CE}^{max} . To prevent irreversible damage to muscle fibres, the maximal
198 MTC length used in experiments is typically not far above the MTC length that yields maximal isometric
199 SEE force (L_{MTC}^{opt}). Accordingly, we simulated quick-release experiments at various initial MTC lengths,
200 ranging from a very short MTC length (i.e., a length yielding very low isometric SEE force) and at every 1
201 mm increment up to a MTC length that was maximal 3 mm above L_{MTC}^{opt} .

202 **Step-ramp experiments** Each step-ramp experiment consisted of an isometric phase slightly above (± 0.5
203 mm) L_{MTC}^{opt} , followed by a rapid (step) change (10 ms) in MTC length and then a constant MTC velocity
204 ramp (see Figure 3B). CE stimulation was maximal (i.e., STIM = 1) during the first isometric phase and
205 continued at this maximal level until it was switched off 0.1 s after the step change in MTC length occurred.
206 The change in MTC length of this step and the constant MTC velocity of the ramp were chosen such that
207 this resulted in a more or less a constant SEE force (and therefore constant CE force) at the beginning of
208 the ramp. We simulated 9 step-ramp experiments with different combinations of step sizes and constant
209 MTC velocity ramps, to cover a substantial part of the concentric CE force-velocity relationship.

210 **Isometric experiments** Isometric experiments were simulated for a combination of different MTC lengths
211 (about 0, -2, -4 and -6 mm below L_{MTC}^{opt}) and stimulation durations (35, 65 and 95 ms). CE stimulation was
212 maximal (i.e., STIM = 1) during the indicated stimulation duration and fully off elsewhere (see Figure 3C).
213 The combination of four different MTC lengths and three different stimulation durations resulted in twelve
214 different isometric experiments.

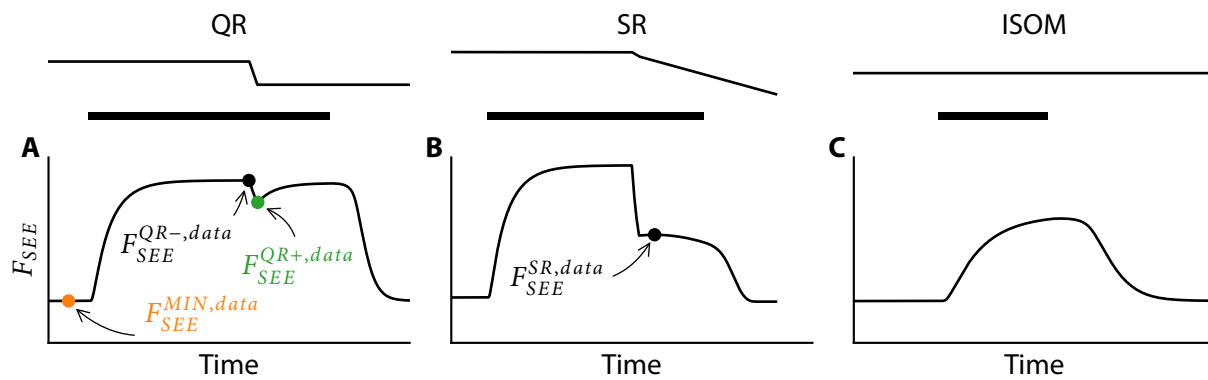


Figure 3: Example of simulated data of quick-release (A), step-ramp (B) and isometric (C) experiments.

Top: MTC length over time. Bottom: SEE force over time. CE stimulation is maximal during the period indicated by the black bar, and ‘off’ elsewhere. For each experiment, we obtained specific datapoints of SEE force and the corresponding MTC length, which were used to estimate contraction and excitation dynamics parameter values.

2.2.2 *In situ* data

We also used data from an *in situ* experiment on isolated rat m. gastrocnemius medialis, conducted on three male Wistar rats. The experiment included quick-release, step-ramp and isometric experiments, which were similar to those described in Section 2.2.1. For each rat, we performed between 11 and 13 quick-release experiments, 10 and 12 step-ramp experiments and 12 isometric experiments. Below, we provide a brief description of the experimental procedure, which is fully detailed in (Reuvers et al., 2025).

In the experiment, approved by the Committee on the Ethics of Animal Experimentation at the Vrije Universiteit (Permit Number: FBW- AVD11200202114471), rats were first anaesthetised with urethane. The hindlimb was then shaved, and the overlying skin and m. biceps femoris were removed. The medial and lateral part of m. gastrocnemius were carefully separated from their surrounding tissue and exposed as much as possible. The rats were placed in the experimental setup with the hindlimb, femur and foot fully fixed. The distal end of the calcaneal tendon was attached to a servomotor (Aurora 309C, Aurora Scientific, Aurora, Canada) using Kevlar thread and aligned to ensure that m. gastrocnemius medialis pulled in its natural direction. All nerves not innervating m. gastrocnemius medialis were severed. M. gastrocnemius medialis was stimulated via a cuff-electrode placed on the sciatic nerve, with the proximal nerves crushed to prevent spinal reflexes. This experimental setup allowed for precise control of m. gastrocnemius medialis length changes and stimulation as well as accurate measurement of m. gastrocnemius medialis force.

2.3 Parameter value estimation procedure

The general procedure to estimate the parameter values involved minimising the sum of squared differences between the data and the values based on the estimated parameter values. To distinguish between these, we used subscripts: for example, the value of the SEE force before the quick-release of the data is indicated by $F_{SEE}^{QR-,data}$ while the value based on the estimated parameter values is indicated by $F_{SEE}^{QR-,est}$.

The data of the quick-release experiments were used to estimate the parameter values of the CE, PEE and

238 SEE force-length relationships. The data of the step-ramp experiments were used to estimate the parameter
 239 values of the CE force-velocity relationship. The data of the isometric experiments were used to estimate
 240 the parameter values of the excitation dynamics. Below we provide an overview on the methods used to
 241 estimate the parameter values. We also offer an open-source toolbox that automates the estimation of
 242 contraction and excitation dynamics parameter values.

243 2.3.1 CE, SEE and PEE force-length parameter value estimation

244 As explained in the introduction, different combinations of contraction dynamics parameters can yield
 245 almost identical mechanical behaviour under isometric conditions (see also Figure 1). For this reason,
 246 it is important to estimate SEE stiffness first, in order to discriminate between SEE stiffness on the one
 247 hand, and L_{CE}^{opt} and L_{SEE}^o on the other. In our approach, the parameter that scales SEE stiffness (k_{SEE}) is
 248 therefore estimated first. This is followed by the estimation of the PEE parameters, as k_{SEE} is also required
 249 for their estimation. Finally, the parameters F_{CE}^{max} , L_{CE}^{opt} , and L_{SEE}^o are estimated.

250 **Estimation of SEE stiffness.** The first step was to estimate SEE stiffness. The model SEE force depends on
 251 the parameter values of k_{SEE} and L_{SEE}^o , and obviously on SEE length. The problem, however, is that SEE
 252 length is unknown in experiments. This makes it challenging to estimate the parameter values concerning
 253 the SEE force-length relationship. Fortunately, quick-release experiments provide a way out. During
 254 quick-release experiments with a servomotor, the motor quickly shortens MTC length such that there is a
 255 rapid decline in SEE force (the ‘quick-release’). Due to the shortness of this timeframe, CE shortening
 256 is minimal such that *almost all* MTC shortening is taken up by SEE. Often, in experimental studies, it is
 257 assumed that *all* MTC shortening can be attributed to SEE shortening. In reality, this assumption leads to
 258 an overestimation of SEE shortening, as CE also shortens during this short timeframe. We introduced a
 259 method to correct for this overestimation of SEE shortening (see Section 2.3.4) and estimated the parameter
 260 values considering both methods: without and with correcting for CE shortening during the quick-release.

261 Obtaining the SEE length change due to the quick-release (ΔL_{SEE}^{QR}) is a crucial step. This is because SEE
 262 length after the quick-release (L_{SEE}^{QR+}) can then be expressed as SEE length before the quick-release (L_{SEE}^{QR-})
 263 plus the change in SEE length due to the quick-release: $L_{SEE}^{QR+} = L_{SEE}^{QR-} + \Delta L_{SEE}^{QR}$. This allowed us to rewrite
 264 Equation 2 to estimate SEE force immediately before ($F_{SEE}^{QR-,est}$) and after ($F_{SEE}^{QR+,est}$) the quick-release. This
 265 yielded:

$$\begin{aligned} F_{SEE}^{QR-,est} &= k_{SEE} \cdot (L_{SEE}^{QR-} - L_{SEE}^o)^2 \\ F_{SEE}^{QR+,est} &= k_{SEE} \cdot (L_{SEE}^{QR-} + \Delta L_{SEE}^{QR} - L_{SEE}^o)^2 \end{aligned} \quad (9)$$

266 Now, there are two unknown parameters (i.e., k_{SEE} and L_{SEE}^o), while also SEE length before the quick-
 267 release is also unknown for each quick-release experiment. Consequently, there are more unknowns than
 268 equations. To address this issue, we replaced $L_{SEE}^{QR-} - L_{SEE}^o$ with a temporary parameter c_{SEE} . This yielded:

$$\begin{aligned} F_{SEE}^{QR-,est} &= k_{SEE} \cdot (c_{SEE})^2 \\ F_{SEE}^{QR+,est} &= k_{SEE} \cdot (c_{SEE} + \Delta L_{SEE}^{QR})^2 \end{aligned} \quad (10)$$

As k_{SEE} scales SEE stiffness, its value is constant across all quick-release experiments. In contrast, c_{SEE} depends on the parameter L_{SEE}^0 and SEE length before the quick-release, which differs among each quick-release experiment. Consequently, c_{SEE} should be determined for each quick-release experiment individually. Visually, c_{SEE} determines the shift along the x-axis on the SEE force-length relationship, while k_{SEE} scales SEE stiffness and consequently SEE force (see Figure 4A). The value of k_{SEE} (and c_{SEE} for each quick-release experiment) were found by minimising the sum of squared differences between the data and estimated SEE force before (F_{SEE}^{QR-}) and after (F_{SEE}^{QR+}) the quick-release.

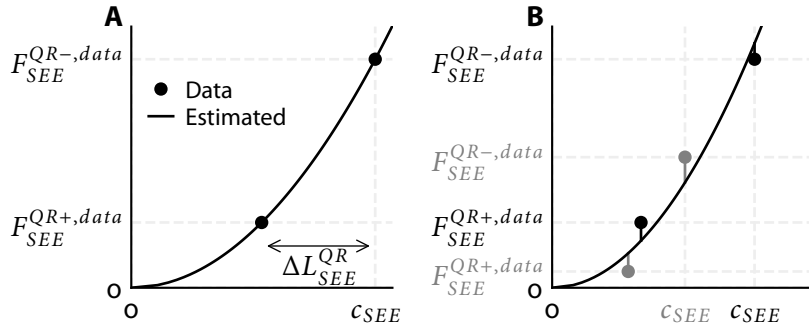


Figure 4: Graphical illustration of SEE stiffness parameter estimation. For each quick-release experiment, SEE force before ($F_{SEE}^{QR-,data}$) and after ($F_{SEE}^{QR+,data}$) the quick-release was obtained from the data, as well as the corresponding decrease in SEE length (ΔL_{SEE}^{QR}). Since SEE length prior to the quick-release is typically unknown, a temporary parameter (c_{SEE}) was introduced for each experiment to represent the difference between SEE length before the quick-release and SEE slack length. A) A single quick-release experiment yields two unknowns: c_{SEE} and a parameter that scales SEE stiffness (k_{SEE}). B) Running multiple quick-release experiments yields $n+1$ unknowns: n values of c_{SEE} (one for each experiment) and the parameter scaling SEE stiffness. Here, two quick-release experiments are illustrated (one indicated with black dots, the other with grey dots), while the estimated SEE force-length relationship is depicted with the black line.

Estimation of PEE parameter values. The second step was to estimate PEE stiffness. The model PEE force depends on the parameter values of k_{PEE} and L_{PEE}^0 , and obviously on PEE length. In experiments, SEE force is measured, while PEE force is required to estimate PEE stiffness. As such, experimental data should be used in which CE force is negligible such that PEE force is approximately equal to SEE force. At the beginning of the quick-release experiments, the active state is so low that CE force is negligible. We selected an interval of 10 ms in which the SEE force was minimal (F_{SEE}^{min} , orange dot in Figure 3A).

In experiments, PEE length is unknown. This problem can be addressed as follows. First, PEE length equals MTC length minus SEE length: $L_{PEE} = L_{MTC} - L_{SEE}$ (Equation 1). Second, SEE length is the sum of SEE slack length and SEE elongation (E_{SEE} : $L_{SEE} = L_{SEE}^0 + E_{SEE}$). This allowed us to rewrite Equation 2 to estimate PEE force (F_{PEE}^{est}), yielding:

$$F_{PEE}^{est} = k_{PEE} \cdot (L_{MTC} - L_{SEE}^0 - E_{SEE} - L_{PEE}^0)^2 \quad (11)$$

Now, there are two unknown parameter values (i.e., k_{PEE} and L_{PEE}^0), while also SEE elongation is unknown for every quick-release experiment. Consequently, there are more unknowns than equations. To address this, we replaced $L_{PEE}^0 + L_{SEE}^0$ with a temporary parameter c_{PEE} . Subsequently, SEE elongation was computed as $\sqrt{\frac{F_{SEE}^{MIN,data}}{k_{SEE}}}$, given the estimated SEE stiffness scaling factor in the previous step. This yielded:

$$F_{PEE}^{est} = k_{PEE} \cdot (L_{MTC} - \sqrt{\frac{F_{SEE}^{MIN,data}}{k_{SEE}} - c_{PEE}})^2 \quad (12)$$

As k_{PEE} only scales PEE stiffness, its value is constant across all quick-release experiments. Similarly, c_{PEE} is the sum of L_{SEE}^0 and L_{PEE}^0 and should therefore be constant for each quick-release experiment. The values of k_{PEE} and c_{PEE} were then computed by minimising the sum of squared differences between F_{PEE}^{est} and $F_{SEE}^{min,data}$.

Estimation of F_{CE}^{max} , L_{CE}^{opt} and L_{SEE}^0 . The third step was to estimate F_{CE}^{max} , L_{CE}^{opt} and L_{SEE}^0 . Before the quick-release, MTC is isometrically delivering force. We used the SEE force at this instant ($F_{SEE}^{QR-,data}$, black dot in Figure 3A) and the corresponding MTC length to obtain the MTC force-length relationship from the data. We then estimated maximal isometric CE force (F_{CE}^{max}), CE optimum length (L_{CE}^{opt}) and SEE slack length (L_{SEE}^0) by minimising the sum of squared differences between the data and estimated MTC force-length relationship. Lastly, L_{PEE}^0 was computed by subtracting L_{SEE}^0 from c_{PEE} .

2.3.2 CE force-velocity parameter value estimation

The values of the CE force–velocity relationship parameters a and b were estimated from data obtained during the plateau phase of SEE force in step-ramp experiments. This approach was chosen because SEE length is constant when SEE force is constant. Consequently, CE velocity equals MTC velocity under these conditions. Following this argument, we first identified a 10 ms interval in which SEE force changed the least. Second, we derived CE length and CE force as functions of time using Equation 1 and Equation 2. Third, we calculated the CE velocity as the time-derivative of CE length. Finally, we averaged CE force and CE velocity over the 10 ms interval. This procedure yielded the data of the CE force-velocity relationship.

Now, the model CE force-velocity relationship can be fit to that of the data to obtain value of a and b . However, employing a method that simply minimises the sum of ordinary least squares differences would not be appropriate because in experiments there is uncertainty in both measured CE force and CE velocity. Instead, we used a total least squares method that minimised the distance between the modelled CE force (F_{CE}^{est}) and CE velocity (v_{CE}^{est}) (now called: model values) and those of the data (see also Figure 5). To do this, we had to find the nearest model values to the CE force of the data (F_{CE}^{data}) and CE velocity of the data (v_{CE}^{data}) (now called: datapoints). We used the following observations: 1) the model value has to satisfy Equation 4 and 2) the derivative of $\frac{dF_{CE}}{dv_{CE}}$ of the model value should be perpendicular to the line from the datapoint to the model value (see Figure 5). Hence, the model value could be found by solving Equation 4 and Equation 13:

$$\frac{dv_{CE}^{est}}{dF_{CE}^{est}} \cdot (v_{CE}^{est} - v_{CE}^{data}) = F_{CE}^{data} - F_{CE}^{est} \quad (13)$$

318 The following cost-function was then minimised to find the parameter values of a and b :

$$J = \sum_{i=1}^n \left(\frac{F_{CE}^{data} - F_{CE}^{est}}{c_1} \right)^2 + \left(\frac{v_{CE}^{data} - v_{CE}^{est}}{c_2} \right)^2$$

319 c_1 and c_2 denote scaling factors such that both terms of the cost-function are more or less equally weighted,
 320 which was done by setting c_1 equal to the maximal range in CE force of the data and setting c_2 equal to the
 321 maximal range of CE velocity of the data.

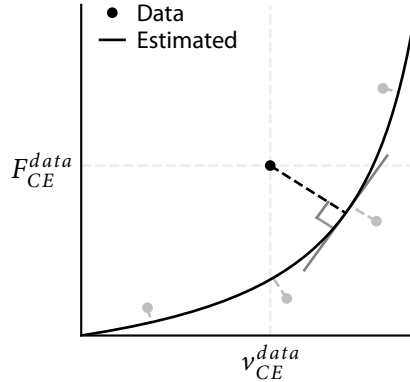


Figure 5: Graphical illustration of the CE force-velocity parameter estimation using total least squares.

For each step-ramp experiment, CE force and CE velocity was obtained during the interval in which SEE force changed the least. The nearest point on the CE force-velocity relationship was identified based on two criteria: it should satisfy Equation 4, and the line from the datapoint to the CE force-velocity relationship should be perpendicular the CE force-velocity relationship. This was done for all step-ramp experiments (other datapoints are depicted in grey), while the estimated CE force-velocity relationship is depicted with the black line.

322 **2.3.3 Excitation dynamics parameter value estimation**

323 We estimated the parameters values of τ_{act} and τ_{deact} based on isometric experiments. The choice to
 324 estimate only these parameters of the excitation dynamics was made because it is generally challenging to
 325 discriminate between parameter values of both the calcium dynamics (Equation 7) and the $q - [Ca^{2+}]$
 326 relation (Equation 8) based on mechanical measurements outlined above. The parameter values of the
 327 $q - [Ca^{2+}]$ relation were set to those used in simulating the isometric experiments. Consequently, these
 328 parameters matched their actual values for the simulated data, but obviously were suboptimal for the *in*
 329 *situ* data. To estimate the parameter values of τ_{act} and τ_{deact} , we minimised the sum of squared differences
 330 between the SEE force of the data and the estimated SEE force based on the parameter values. For this, an
 331 interval of the data was used starting from maximal CE stimulation to 0.1 s after CE stimulation ceased off.

332 **2.3.4 Parameter estimation: traditional method & improved method**

333 To estimate the SEE stiffness it is generally assumed that the quick-release is so fast that all MTC shortening
 334 is taken up by SEE. As A.V. Hill already acknowledged in (1950), this is not the case in reality as CE also
 335 shortens. Although this CE shortening might be small, SEE is in general stiff and therefore small errors

in SEE length may result in large errors in predicted SEE forces and thus in estimated SEE stiffness. We used two different methods to estimate the parameter values: 1) the traditional method and the improved method. In the traditional method, we followed the procedure outlined in section Section 2.3.1 and Section 2.3.2. In the improved method, we also followed the procedure outlined in Section 2.3.1 and Section 2.3.2 after which we incorporated an additional procedure to correct for CE shortening due to the quick-release. This additional procedure was as follows: 1) We calculated CE length just before the (step) change in MTC length occurred using Equation 1, 2, 3 and 8, assuming that CE velocity was 0 and that γ equalled 1. 2) We performed a (short) simulation from the time just before the (step) change in MTC length to just after the (step) change in MTC length. 3) We computed the change in CE length over this time interval as the average CE length slightly before and slightly after the (step) change in MTC length. 4) We subtracted the change in CE length from the change in MTC length to obtain the change in SEE length. In addition to correcting for CE length change during the quick-release, we incorporated a step to obtain better estimates of the actual PEE force at the time instance of minimum SEE force ($F_{SEE}^{min,data}$; see Figure 3). We computed CE force at this time instance using Equation 3 and 8, assuming that γ equalled its minimum value. This CE force was then subtracted from $F_{SEE}^{min,data}$.
The improved method leads to a different (i.e., higher) SEE stiffness, which affect the estimation of the parameter values of the CE, PEE and SEE force-length relationships (see Section 2.3.1). These estimated parameter values were then used to again estimate the parameter values of the CE force-velocity relationship (see section Section 2.3.2). As the parameter values of the CE force-velocity relationship slightly changed, the estimate of CE length change due to the quick-release also changed and therefore estimated SEE stiffness changed. We found that this process always converged to a stable solution and therefore we used an iterative process until the change in all parameter values was less than 0.1% (see Figure S2).

2.4 Sensitivity analysis

2.4.1 Monte Carlo simulations

In experiments on isolated MTC, the MTC force-length relationship can shift due to irreversible damage of SEE (Aubert et al., 1951). We observed this phenomenon in an experiment involving isolated rat m. gastrocnemius medialis, where the MTC force-length relationship shifted by about 1 mm ($\sim 8\% L_{CE}^{opt}$) over a period of approximately 8 hours (Reuvers et al., unpublished observation). To assess the influence of these shifts on the parameter value estimation, we performed Monte Carlo simulations. We assumed that the observed shifts of the MTC force-length relationship were caused solely by a decrease in SEE stiffness. Accordingly, we decreased SEE stiffness to cause random shifts of the MTC force-length relationship between 0 and 1 mm. This way, we simulated data as if they were collected at random intervals throughout an 8-hour period. Importantly, changes in SEE stiffness affect the step size and constant MTC velocity ramp required for a more or less a constant SEE force at the beginning of the ramp in step-ramp experiments. Therefore, we adjusted the step size and constant MTC velocity ramp for each simulated step-ramp trial individually. Parameter values of each MTC were then estimated using the ‘perturbed’ data using the improved method (see Section 2.3.4). This process was repeated 50 times for each MTC, allowing us to evaluate both the mean and the spread of the estimated parameter values.

374 **2.4.2 Interdependency of parameter values**

375 The parameter estimation procedure detailed above follows a fixed order in which certain parameters
376 are estimated before others. For instance, k_{SEE} is estimated first and therefore affects the estimation of
377 L_{SEE}^0 and L_{CE}^{opt} . This sequence creates an interdependency among the parameter values, which has been
378 identified as a potential cause for substantial variation in parameter values among individuals, even within
379 the same muscle type (Lemaire et al., 2016). To investigate this interdependency, we systematically changed
380 parameter values of our model. Specifically, we increased and decreased each parameter value by 5%
381 relative to the values obtained with the improved method. After this, we re-estimated all other parameter
382 values. This approach allowed us to assess the influence of changes in one parameter on the estimation of
383 others.

384 **3 Results**

385 **3.1 Evaluating parameter value estimation accuracy - simulated data**

386 **3.1.1 Traditional method versus Improved method**

387 The traditional method did not correct for CE shortening during quick-release experiments. Consequently,
388 SEE shortening due to the quick-release was overestimated by 24% on average. This overestimation of
389 SEE shortening caused a decrease in k_{SEE} (and thus SEE stiffness) of 34% on average. The estimation
390 of the activation time constant was most affected by the underestimated SEE stiffness, resulting in an
391 underestimation of 19% on average. All other estimated parameter values were within 9% of their actual
392 values (Table 1). These findings show the influence of CE shortening — even within a very brief 10 ms
393 interval — on the parameter value estimation of both the contraction dynamics and excitation dynamics.

394 In contrast, the improved method corrected for CE shortening during the quick-release experiments. The
395 correction substantially reduced the overestimation of SEE shortening, yielding an accurate estimate of
396 k_{SEE} . As a result, all estimated parameter values deviated by no more than 3% from their actual values
397 (Table 1). These results demonstrate that accounting for CE shortening - even over a brief 10 ms interval -
398 substantially improves the accuracy of the parameter value estimation.

399 For interested readers, we discuss below the specific factors contributing to the differences between the
400 actual contraction and excitation dynamics parameter values and those estimated based on the traditional
401 method.

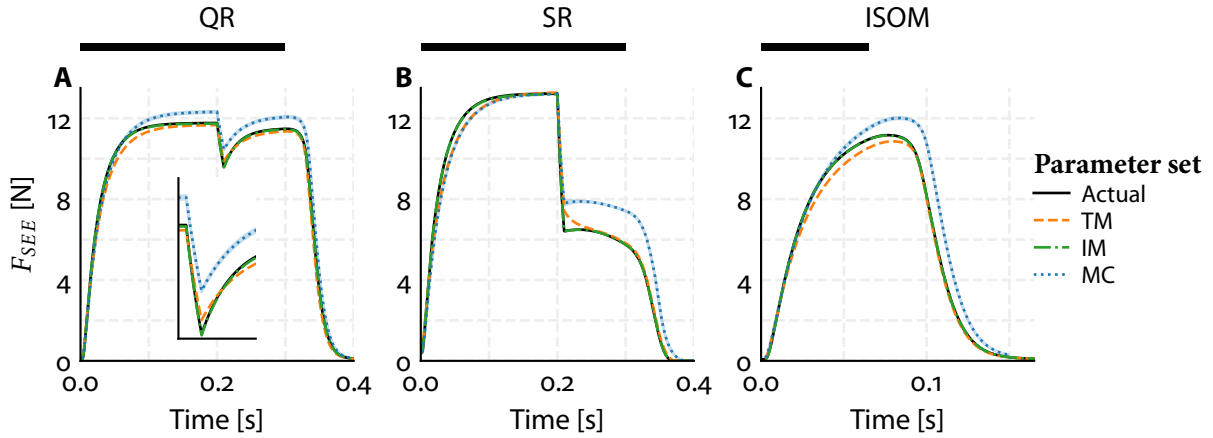


Figure 6: Representative example of SEE force over time during a quick-release (A), step-ramp (B) and isometric experiment (C). The inset in (A) depicts the SEE force over time around the quick-release. The SEE force over time is depicted for four sets of parameter values: 1) the actual values (i.e., literature-obtained; black solid line), those obtained with the traditional method (TM; orange dashed line), those obtained with the improved method (IM; green dashed-dotted line) and those resulting from the Monte Carlo Simulations (MC; blue dotted line, with shaded 95% confidence interval).

Table 1: Percentage differences between estimated and actual MTC parameter values.

| | Traditional method | | | Improved method | | | Monte Carlo | | |
|----------------|--------------------|-----------------|-----------------|-----------------|-----------------|-----------------|-----------------|-----------------|-----------------|
| | GM ₁ | GM ₂ | GM ₃ | GM ₁ | GM ₂ | GM ₃ | GM ₁ | GM ₂ | GM ₃ |
| a | 1 | 4 | 2 | 1 | 3 | 1 | 1 ± 2 | 6 ± 2 | 2 ± 3 |
| b | -0 | 2 | -1 | 1 | 2 | 1 | 1 ± 2 | 5 ± 2 | 2 ± 3 |
| F_{CE}^{max} | 0 | -1 | 0 | -0 | -1 | -0 | -0 ± 1 | -2 ± 1 | -1 ± 1 |
| k_{PEE} | 3 | -9 | 9 | -0 | 0 | -0 | 3 ± 17 | 3 ± 15 | 7 ± 31 |
| k_{SEE} | -39 | -27 | -37 | 0 | -1 | 0 | -37 ± 6 | -36 ± 6 | -35 ± 6 |
| L_{CE}^{opt} | -1 | -2 | -3 | -0 | 0 | -0 | 0 ± 3 | 1 ± 3 | 0 ± 3 |
| L_{PEE}^o | 0 | -1 | -0 | -0 | 0 | -0 | 0 ± 3 | 1 ± 2 | 0 ± 2 |
| L_{SEE}^o | -1 | -0 | -0 | 0 | -0 | 0 | -0 ± 1 | -0 ± 1 | -0 ± 1 |
| τ_{act} | -21 | -16 | -21 | -0 | -1 | -0 | 1 ± 3 | 1 ± 4 | 1 ± 4 |
| τ_{deact} | -5 | -4 | -5 | 0 | 0 | 0 | 0 ± 1 | 0 ± 1 | 0 ± 1 |

402 3.1.2 Understanding errors in parameter value estimation

403 **Estimation of SEE stiffness.** The SEE stiffness parameter (k_{SEE}) was underestimated by 39%, 27% and
 404 37% for GM₁, GM₂ and GM₃, respectively (see Table 1). This overestimation directly resulted from the
 405 overestimation of SEE shortening due to the quick-release, which was overestimated by 28±2%, 17±2% and

406 26±2% for GM1, GM2 and GM3, respectively, averaged across all quick-release experiments. In absolute
407 terms, CE shortened only 43±3, 29±2 and 41±2 µm over the 11 ms interval between the time points at
408 which SEE force and SEE length were sampled (i.e., immediately before and after the quick-release). The
409 amount of CE shortening was smallest in GM2 because GM2 was a slower muscle than GM1 and GM3.
410 Consequently, the overestimation of SEE shortening was also smallest in GM2, which in turn led to the
411 smallest underestimation of k_{SEE} . All in all, this shows that even very small amounts of CE shortening has
412 substantial influence on the estimation of SEE stiffness.

413 Since SEE was very stiff, the overestimation in SEE elongation at maximal isometric CE force was only
414 0.50, 0.32 and 0.49 mm for GM1, GM2 and GM3, respectively. This is an important finding because the
415 SEE stiffness is the first parameter in the estimation process and therefore affects all subsequent estimated
416 parameter values. Therefore, since the overestimation of SEE elongation (in mm) at maximal isometric CE
417 force was only small, the impact on the estimation of the other contraction dynamics parameter values
418 was also small.

419 Lastly, it should be noted that the correlation coefficient between the data SEE force-length relationship and
420 the one based from the estimated parameters is not an adequate measure of how accurately SEE stiffness
421 is captured. Obviously, a correlation coefficient is not sensitive to the overestimation of SEE shortening
422 due to the quick-release. Consequently, high correlation coefficients ($R^2 > 0.99$) can still be observed
423 even when SEE stiffness is substantially underestimated. To further investigate this issue, we simulated
424 the quick-release experiments after obtaining all contraction and excitation dynamics parameter values.
425 The simulations clearly showed a slower rise in SEE force after the quick-release in comparison with the
426 experimental data (Figure 6A), indicating that SEE stiffness was underestimated. These results suggest
427 that the rise in SEE force is a better measure of SEE stiffness estimation accuracy.

428 **Estimation of PEE parameter values.** The PEE stiffness parameter (k_{PEE}) was 2.8% higher, 8.6% lower
429 and 8.7% higher than the actual parameter value for GM1, GM2 and GM3, respectively (see Table 1). PEE
430 slack length (L_{PEE}^0) values were 0.29% higher, 1.4% lower and 0.048% lower than the actual values for GM1,
431 GM2 and GM3, respectively (see Table 1). The available data to estimate $E_{PEE}^{max,rel}$ and L_{PEE}^0 was limited as
432 in most quick-release experiments PEE length was below L_{PEE}^0 . In fact, only 4, 4 and 3 datapoints were
433 used to estimate the PEE force-length relationship for GM1, GM2 and GM3, respectively. Notwithstanding,
434 the estimated PEE parameter values were within 8.7% of their actual value.

435 **Estimation of F_{CE}^{max} , L_{CE}^{opt} and L_{SEE}^0 .** The estimated values of F_{CE}^{max} , L_{CE}^{opt} , and L_{SEE}^0 were within 2.6% of
436 their actual values (see Table 1). The deviations were all due to the underestimation of k_{SEE} , which can
437 be explained in detail as follows. First, the width of the model's MTC force-length relationship is mainly
438 determined by k_{SEE} and L_{CE}^{opt} . The lower k_{SEE} , the wider the MTC force-length relationship; the shorter
439 L_{CE}^{opt} , the narrower the relationship. Consequently, underestimating k_{SEE} caused a underestimation of L_{CE}^{opt} .
440 Second, a lower L_{CE}^{opt} results in a lower L_{MTC}^{opt} . This led to L_{SEE}^0 being overestimated such that L_{MTC}^{opt} of the
441 data and model were aligned. Third, a lower k_{SEE} , lower L_{CE}^{opt} and higher L_{SEE}^0 results in a narrower MTC
442 force-length relationship (see Figure 1A). This resulted in an increase F_{CE}^{max} in order to minimise the root
443 mean squared distance between estimated MTC force-length relationship and that of the data. Therefore,

444 the underestimation of SEE stiffness resulted in a small overestimation of F_{CE}^{max} , and L_{SEE}^o , and a small
445 underestimation of L_{CE}^{opt} .

446 **Estimation of CE force-velocity parameter values.** The estimated value of a was overestimated by up
447 to 3.8%, while b was within 1.6% of its actual value (see Table 1). The slight overestimation of a resulted
448 from the estimation of CE force and CE velocity over a 10 ms interval in which the SEE force changed the
449 least (see Figure 3B). At high shortening velocities, CE length decreased so rapidly that — even over a
450 short interval of 10 ms — SEE force changed. Consequently, assuming that CE velocity equalled MTC
451 velocity led to an overestimation of CE velocity. These findings show that it is crucial in experiments to
452 find a combination of step sizes and constant MTC velocity ramps resulting in a nearly constant SEE force.
453 While this is experimentally challenging, achieving this would allow for accurate estimation of the CE
454 force-velocity relationship.

455 **Estimation of excitation dynamics parameter values.** τ_{act} and τ_{deact} were underestimated across all
456 muscles. For GM1, GM2, and GM3, τ_{act} was underestimated by 21%, 16% and 21%, respectively, while
457 τ_{deact} was underestimated by 4.9%, 3.6% and 5.1%, respectively (see Table 1). This underestimation was
458 primarily due to the underestimation of SEE stiffness. In short, the underestimation of SEE stiffness caused
459 an overestimation of SEE lengthening velocity, which in turn lead to an overestimation of CE shortening
460 velocity. This reduced CE force via the CE force-velocity relationship and therefore a slower increase in SEE
461 force. Consequently, τ_{act} was overestimated, leading to faster increase in SEE force. The underestimation
462 of τ_{act} also resulted in an overestimation of the relative $[Ca^{2+}]$ at the start of the deactivation, causing a
463 decrease in τ_{deact} (leading to a faster decrease in SEE force). This finding highlights the influence of the
464 contraction dynamics on the estimation of the excitation dynamics parameter values.

465 To illustrate the influence of the contraction dynamics on the estimation of the excitation dynamics
466 parameter values, we also fitted τ_{act} and τ_{deact} to the data of the quick-release and step-ramp experiments.
467 Using the quick-release data, τ_{act} was underestimated by 38% on average and based on step-ramp data τ_{act}
468 was underestimated by 64% on average. In turn, τ_{deact} was underestimated by only 1% on average for both
469 data sets. These results show that quick-release and step-ramp experiments are not suitable for accurately
470 estimating τ_{act} due to substantial CE length changes that occur in these experiments. To minimise the
471 influence of contraction dynamics and improve the estimation of τ_{act} , experiments should be performed
472 in which CE length changes are minimal. Isometric experiments are best suited for this purpose.

473 3.2 Sensitivity analysis

474 3.2.1 Monte Carlo simulations

475 Monte Carlo simulations were used to examine how shifts in the MTC force-length relationship caused by
476 a decrease in SEE stiffness (e.g., due to irreversible SEE damage in experiments) affect the accuracy of the
477 estimated contraction and excitation dynamics parameter values. The induced shifts of the MTC force-
478 length relationship were between 0–1 mm, and therefore it was no surprise that SEE stiffness decreased by
479 36% on average — which corresponds to a 0.5 mm shift.

480 All other estimated contraction dynamics parameter values were within 6.3% on average of their actual

481 value (Table 1). The variance in the estimated contraction dynamics parameter values was below 31%
482 for all parameters except for the PEE stiffness scaling parameter. The PEE stiffness scaling parameter
483 showed substantially higher variance (with a standard deviation up to 31%), because it was based on
484 four or fewer quick-release trials, making it more sensitive to perturbations in the data. Regarding the
485 excitation dynamics, the influence on the average time constants was minimal (within 0.71%), but affected
486 the variance in the estimated values of the activation time constant (with a standard deviation of 4% on
487 average). These findings indicate that an average decrease in SEE stiffness of 36% has a much smaller effect
488 on the estimated parameter values of the contraction and excitation dynamics, even at the level of an
489 individual muscle.

490 3.2.2 Interdependency of parameter values

491 We investigated the interdependency of the estimated parameter values by adjusting each parameter value
492 by 5% and re-estimating all other parameter values. F_{CE}^{max} and L_{SEE}^o were the parameters that had most
493 effect on the estimates of the others.

494 First, F_{CE}^{max} affected the estimation of parameter a and b of the CE force-velocity relationship. Under-
495 estimating F_{CE}^{max} leads to an underestimation of CE force at o velocity. Due to the formulation of the
496 CE force-velocity relationship, the curve, by definition, crosses the point at $v_{CE} = 0$ and $F_{CE} = F_{CE}^{max}$.
497 Consequently, the best fit to the data with an underestimated F_{CE}^{max} is a much flatter CE force-velocity
498 relationship, which is realised by an increase in a and a decrease in b . This flatter CE force-velocity
499 relationship affects the estimation of all other contraction dynamics parameter values because the CE
500 force-velocity relationship is used to estimate the CE shortening due to the quick-release (see Section 2.3.4).
501 As a result, k_{SEE} and L_{SEE}^o decreased due to underestimating F_{CE}^{max} , whereas L_{CE}^{opt} increased. In summary,
502 F_{CE}^{max} substantially influenced the estimation of all contraction dynamics parameter values mainly by its
503 effect on the CE force-velocity relationship.

504 Second, L_{SEE}^o affected the estimation of L_{CE}^{opt} and F_{CE}^{max} . As explained earlier, when L_{SEE}^o is overestimated,
505 L_{CE}^{opt} is underestimated, such that L_{MTC}^{opt} remains more or less unaffected. Underestimating L_{CE}^{opt} causes
506 a narrower MTC force-length relationship, leading to an overestimation of F_{CE}^{max} to preserve a good fit
507 between the data and the model. As previously discussed, overestimating F_{CE}^{max} , in turn, resulted in
508 an underestimation of parameters a and b . Thus, L_{SEE}^o substantially influenced the estimation of all
509 contraction dynamics parameter values mainly by its effect on the MTC force-length relationship.

510 Taken together, the interdependence of F_{CE}^{max} and L_{SEE}^o with other parameter values underscores the need
511 for precise estimation of these key parameters. In this regard, it is reassuring that these two parameters
512 were found to be robust for perturbations in the experimental data.

513 3.3 Evaluating model predictions - *in situ* data

514 We estimated contraction and excitation dynamics parameter values from *in situ* data of rat m. gas-
515 trocnemius medialis (Table S2). The improved method yielded a 67% higher SEE stiffness compared to
516 the traditional method. As explained earlier, higher SEE stiffness also affects the estimation of all other
517 parameter values. The most noticeable changes were longer time constants for both the activation (τ_{act})

Table 2: Interdependency of the estimated MTC parameter values. Each entry shows the percentage change in the row parameter resulting from a 5% change in the column parameter. All values are expressed as percentage changes.

| | <i>a</i> | <i>b</i> | F_{CE}^{max} | k_{SEE} | L_{CE}^{opt} | L_{SEE}^o |
|----------------|----------------|----------------|-----------------|----------------|----------------|-----------------|
| <i>a</i> | - | 10.2 ± 1.1 | -14.1 ± 1.7 | -0.1 ± 0.0 | 3.4 ± 0.4 | -10.3 ± 1.5 |
| <i>b</i> | 2.3 ± 0.2 | - | -14.2 ± 2.0 | 0.1 ± 0.0 | 3.8 ± 0.5 | -10.7 ± 1.3 |
| F_{CE}^{max} | -0.0 ± 0.0 | -0.0 ± 0.0 | - | -0.1 ± 0.0 | -1.2 ± 0.2 | 3.6 ± 0.8 |
| k_{PEE} | -0.2 ± 0.1 | -0.4 ± 0.1 | 2.2 ± 0.5 | -1.3 ± 0.4 | -0.5 ± 0.1 | 1.4 ± 0.3 |
| k_{SEE} | 0.6 ± 0.2 | 1.5 ± 0.3 | -6.5 ± 2.1 | - | 1.6 ± 0.4 | -4.2 ± 1.1 |
| L_{CE}^{opt} | 0.0 ± 0.0 | 0.0 ± 0.0 | -5.3 ± 0.6 | 0.2 ± 0.1 | - | -14.0 ± 1.3 |
| L_{PEE}^o | 0.0 ± 0.0 | 0.0 ± 0.0 | 0.0 ± 0.0 | 0.0 ± 0.0 | 0.0 ± 0.0 | -10.5 ± 0.7 |
| L_{SEE}^o | 0.0 ± 0.0 | 0.0 ± 0.0 | 1.8 ± 0.3 | 0.1 ± 0.0 | -1.7 ± 0.1 | - |
| τ_{act} | 0.6 ± 0.2 | 1.6 ± 0.2 | -3.3 ± 1.1 | 2.3 ± 0.2 | 1.1 ± 0.6 | -3.5 ± 2.6 |
| τ_{deact} | 0.2 ± 0.0 | 0.5 ± 0.0 | -2.9 ± 0.2 | 0.6 ± 0.0 | 1.2 ± 0.0 | -2.8 ± 0.3 |

and deactivation (τ_{deact}) dynamics, with increases of 61% and 16% on average, respectively. Another noticeable change was in CE optimum length, which was about 11% higher using the improved method compared to the traditional method.

To assess model predictions, we re-ran quick-release, step-ramp and isometric experiments, as well as stretch-shortening cycles with experimentally measured MTC length and CE stimulation over time as inputs to the model. We compared the model predictions using parameter sets obtained from both methods. For all experiments and rats, the average difference between experimental data and model predictions was 30% smaller on average using parameters from the improved method (Figure 8; Table S3). Overall, the improved method substantially enhanced the predictions derived by the Hill-type MTC model compared to the traditional method.

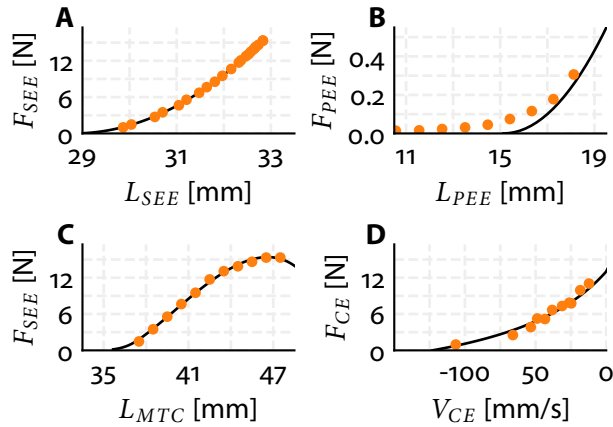


Figure 7: Representative example of experimental *in situ* data of rat 1 for the SEE force-length relationship (A), PEE force-length relationship (B), MTC force-length relationship (C) and the CE force-velocity relationship (D). The orange dots depicts the experimental *in situ* data and the solid black line depicts the model fit.

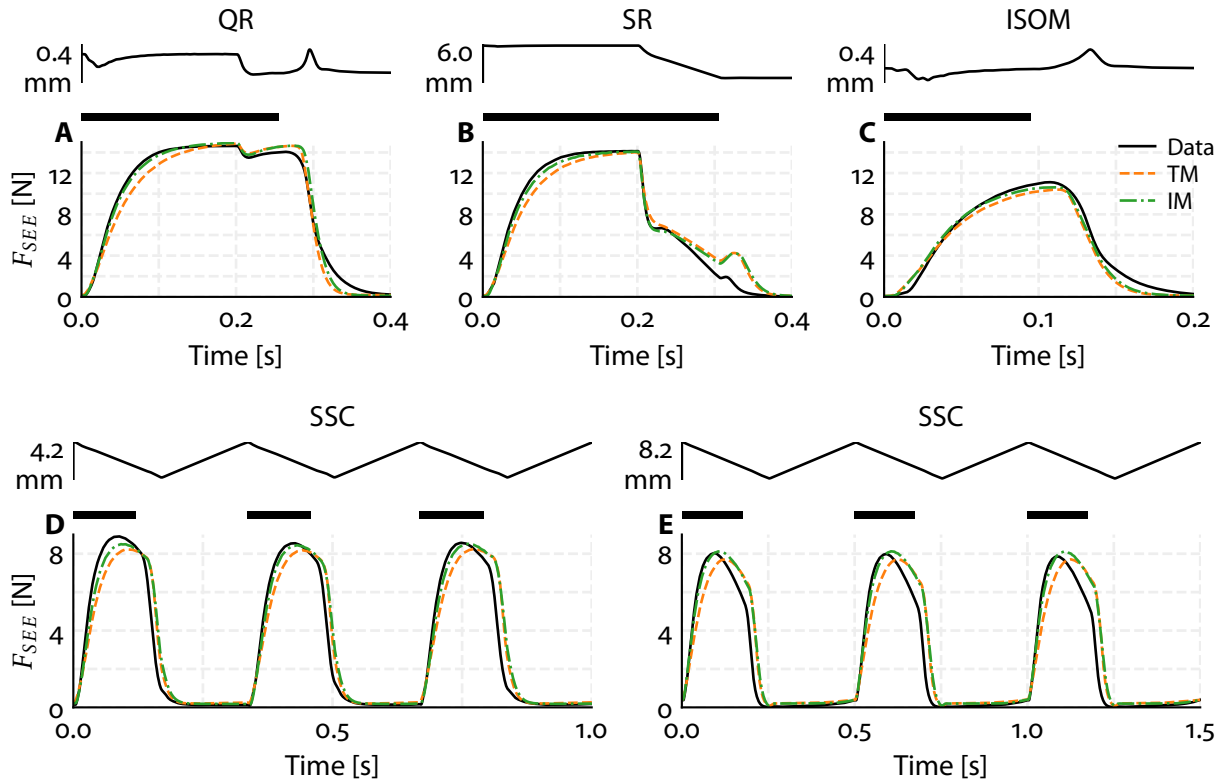


Figure 8: Representative example of experimental *in situ* data and simulation results of rat 1 for SEE force over time during a quick-release experiment (A), step-ramp experiment (B), isometric experiment (C) and two stretch-shortening cycles (D & E). The simulation results were obtained by re-simulating the experimental protocol with the MTC length and CE stimulation from the experimental data as input and by using either the parameter set obtained with the traditional method (TM; orange dashed line) or the improved method (IM; green dash-dotted line). For each panel, the top plot represents MTC length over time, with the bar indicating its range in mm. CE stimulation is maximal during the periods indicated by the black bars and is 'off' elsewhere.

528 4 Discussion

529 The aim of this study was to evaluate the accuracy of estimating contraction and excitation dynamics
 530 parameter values on the basis of data collected in commonly used experimental protocols. In real
 531 experiments, the actual parameter values are unknown, making it impossible to directly assess estimation
 532 accuracy. In this study, we took a different approach: using a Hill-type MTC model with parameter values
 533 obtained from literature we generated synthetic 'data' by simulating quick-release, step-ramp, and isometric
 534 experiments. We then estimated all important contraction and excitation dynamics parameter values
 535 by using the synthetic data. Since the actual parameter values were known in this case, we could assess
 536 how accurately they were retrieved. Two different estimation methods were compared. The first was the
 537 traditional method, commonly used in the literature, which does not account for muscle fibre shortening
 538 during quick-release experiments. The second was an improved method that includes a correction for
 539 muscle fibre shortening during the quick release. Both methods developed in this study—designed to
 540 estimate contraction and excitation dynamics parameters from quick-release, step-ramp, and isometric

541 experiments using servomotors—are made available as an open-source toolbox. In the remainder of this
542 paper, we will discuss 1) the difference between the two methods; 2) the robustness of the improved method
543 and 3) the implications for muscle modelling.

544 In quick-release experiments using servomotors, muscle fibres shorten, even within the short duration of
545 the release. Obviously, the extent of muscle fibre shortening depends on the duration of the quick-release.
546 Consequently, the longer the quick-release, the more important it becomes to account for muscle fibre
547 shortening when estimating SEE stiffness (see Figure S3). For a typical quick-release duration of 10 ms, we
548 found that muscle fibre shortening was nearly 25% of MTC shortening (and thus 33% of SEE shortening),
549 resulting in an underestimation of SEE stiffness by approximately 35%. This finding is important, especially
550 in studies aiming to estimate SEE energy storage from SEE force or length, since energy storage estimates
551 scale linearly with SEE stiffness. Although SEE was substantially underestimated with the traditional
552 method, this had minimal effect on the estimated parameter values of the PEE and CE force-length
553 relationships and the CE force-velocity relationship, but impacted the estimated excitation dynamics
554 parameter values. The improved method, in turn, yielded SEE stiffness values close to the actual ones and
555 substantially enhanced the estimates of the other parameter values.

556 Our sensitivity analysis revealed substantial interdependencies between certain parameters. Particularly,
557 we observed high sensitivity of estimated parameter values to variations in the maximal isometric CE
558 force (F_{CE}^{max}) and the SEE slack length (L_{SEE}^0) parameter values. Despite this sensitivity, it is important to
559 note that these parameters were accurately estimated even from perturbed experimental data. This was
560 true in general: contraction and excitation dynamics parameter values were quite robust against shifts in
561 the MTC force-length relationship of the simulated data according to the Monte Carlo simulations. These
562 findings indicate the robustness of the improved method.

563 We applied both the traditional and the improved method to *in situ* data from quick-release, step-ramp,
564 and isometric experiments on rat m. gastrocnemius medialis. The improved method yielded substantially
565 higher estimates of SEE stiffness compared to the traditional method (67% on average). Using parameter
566 sets from both methods, we simulated the quick-release, step-ramp, and isometric experiments, as well as
567 independent stretch-shortening cycles, all with experimentally obtained MTC length and CE stimulation
568 over time as input to the model. With parameter estimates obtained with the traditional method, the
569 root mean squared difference between predicted and experimentally measured force was about 5.6% of
570 maximal CE force, averaged across all rats and experiments; with parameter estimates obtained with the
571 improved method this was only 3.9%. The small difference between predicted and experimentally observed
572 force over time with parameters from the improved method suggests that muscle force can be accurately
573 predicted with a Hill-type MTC model across a wide variety of contractions. This is a remarkable finding
574 for two reasons. First, the Hill-type MTC model is obviously a simplification of real muscle, abstracting the
575 muscle belly, aponeurosis, and tendon into the CE, SEE, and PEE components, and thus does not account
576 for certain complexities (e.g., non-constant pennation angle, muscle inhomogeneities, etc.). Second, the
577 Hill-type MTC model used in this study consists of 26 parameters, of which only 10 values were estimated.
578 This means that all other parameters were left suboptimal. Despite these simplifications, the model was

579 able to accurately predict muscle behaviour, demonstrating that a relatively simple model with a limited
580 number of estimated parameter values can still capture important aspects of muscle dynamics.

581 In conclusion, our results demonstrate that the improved parameter estimation method provides accurate
582 and robust estimates of contraction and excitation dynamics properties, offering a reliable approach for
583 muscle property estimation in both biomechanical and muscle physiology research. The approach that we
584 designed in this study is made available as an open-source toolbox (<https://github.com/edwinreuvers/mp-estimator>).
585

586 **Acknowledgments**

587 The authors thank Maarten F. Bobbert for helpful comments on a draft of the paper. The authors also
588 thank Koen K. Lemaire for insightful discussions.

589 **Funding**

590 This work was funded by The Dutch Research Council (NWO) [21728 to D.A.K.].

591 **Data and resource availability**

592 All data, code, and materials used in this study are openly available:

- 593 • **GitHub repository:** All raw data, processed data, and analysis code are hosted on GitHub at
594 <https://github.com/edwinreuvers/acc-mp-estimation>.
- 595 • **Reproducible analysis website:** Full analysis pipeline — including data, analysis code, and fig-
596 ure/table generation — is available at <https://edwinreuvers.github.io/publications/acc-mp->
597 [estimation](https://edwinreuvers.github.io/publications/acc-mp-estimation).

598 **Glossary**

| Symbol | Description |
|-------------------|--|
| a | Hill constant |
| b | Hill constant |
| b_{min}^{scale} | Minimal scale factor of b (i.e., the minimal value of b_{scale}) |
| b_{shape} | Determines the steepness of the relation between b_{scale} and q |
| F_{asympt} | Oblique asymptote of the eccentric part of the CE force-velocity relationship |
| F_{CE}^{max} | Maximum isometric CE force |
| k_{PEE} | Scales the PEE stiffness |
| k_{SEE} | Scales the SEE stiffness |
| L_{CE}^{opt} | CE length at which CE can produce maximal isometric force |
| L_{PEE}^o | PEE slack length |
| L_{SEE}^o | SEE slack length |
| r_{as} | Slope of the slanted asymptote of the eccentric part of the CE force-velocity relationship |
| r_{slope} | Ratio between the eccentric and concentric derivatives of $\frac{dF_{CE}^{rel}}{dv_{CE}^{rel}}$ @ $v_{CE} = 0$ |
| w | Determines the width of the CE force-length relationship |
| a_{act} | Determines the steepness of the relation between γ and q |
| $b_{act,1}$ | Determines together with $b_{act,1}$ and $b_{act,3}$ the pCa^{2+} level at which $q = 0.5$ |
| $b_{act,2}$ | Determines together with $b_{act,2}$ and $b_{act,3}$ the pCa^{2+} level at which $q = 0.5$ |
| $b_{act,3}$ | Determines together with $b_{act,1}$ and $b_{act,2}$ the pCa^{2+} level at which $q = 0.5$ |
| k_{Ca} | Relates γ to the actual Ca^{2+} concentration |
| γ_o | Minimal value of γ |
| q_o | Minimal value q |
| τ_{act} | Activation time constant of the calcium dynamics |
| τ_{deact} | Deactivation time constant of the calcium dynamics |

599 References

- 600 **Aubert, X., Roquet, M. L. and Van der Elst, J.** (1951). [The tension-length diagram of the frog's sartorius](#)
601 [muscle. Archives Internationales de Physiologie](#) **59**, 239–241.
- 602 **Blix, M.** (1892). [Die lange und die spannung des muskels. Skandinavisches Archiv Für Physiologie](#) **3**,
603 295–318.
- 604 **Blix, M.** (1893). [Die lange und die spannung des muskels. Skandinavisches Archiv Für Physiologie](#) **4**,
605 399–409.
- 606 **Blümel, M., Hooper, S. L., Guschlbauer, C., White, W. E. and Büschges, A.** (2012). Determining all
607 parameters necessary to build hill-type muscle models from experiments on single muscles. *Biological*
608 *Cybernetics* **106**, 543–548.
- 609 **Bobbert, M. F., Ettema, G. C. and Huijing, P. A.** (1990). [The force-length relationship of a muscle-tendon](#)
610 [complex: experimental results and model calculations. European Journal of Applied Physiology and](#)
611 [Occupational Physiology](#) **61**, 323–329.
- 612 **Bortolotto, S. K., Cellini, M., Stephenson, D. G. and Stephenson, G. M. M.** (2000). [MHC isoform](#)
613 [composition and Ca₂₊- or Sr₂₊-activation properties of rat skeletal muscle fibers. American Journal of](#)
614 [Physiology-Cell Physiology](#) **279**, C1564–C1577.
- 615 **Burkholder, T. J. and Lieber, R. L.** (2001). [Sarcomere length operating range of vertebrate muscles during](#)
616 [movement. Journal of Experimental Biology](#) **204**, 1529–1536.
- 617 **Cecchi, G., Colomo, F. and Lombard, V.** (1978). [Force-velocity relation in normal and nitrate-treated](#)
618 [frog single muscle fibres during rise of tension in an isometric tetanus. The Journal of Physiology](#) **285**,
619 257–273.
- 620 **Ebashi, S. and Endo, M.** (1968). [Calcium and muscle contraction. Progress in Biophysics and Molecular](#)
621 [Biology](#) **18**.
- 622 **Gordon, A. M., Huxley, A. F. and Julian, F. J.** (1966). [The variation in isometric tension with sarcomere](#)
623 [length in vertebrate muscle fibres. The Journal of Physiology](#) **184**, 170–192.
- 624 **Hatze, H.** (1981). *Myocybernetic control models of skeletal muscle*. Pretoria: University of South Africa.
- 625 **Hill, A. V.** (1925). [Length of muscle, and the heat and tension developed in an isometric contraction. The](#)
626 [Journal of Physiology](#) **60**, 237–263.

- 627 Hill, A. V. (1938). **The heat of shortening and the dynamic constants of muscle**. *Proceedings of the Royal
628 Society of London. Series B - Biological Sciences* **126**, 136–195.
- 629 Hill, A. V. (1950). **The series elastic component of muscle**. *Proceedings of the Royal Society of London.
630 Series B - Biological Sciences* **887**, 273–280.
- 631 Katz, B. (1939). The relation between force and speed in muscular contraction. *The Journal of Physiology*
632 **96**, 45–64.
- 633 Kistemaker, D. A., Van Soest, A. J. and Bobbert, M. F. (2005). **Length-dependent [Ca₂₊] sensitivity adds
634 stiffness to muscle**. *Journal of Biomechanics* **38**, 1816–1821.
- 635 Kistemaker, D. A., Terwiel, T. M., Reuvers, E. D. H. M. and Bobbert, M. F. (2023). **Limiting radial pedal
636 forces greatly reduces maximal power output and efficiency in sprint cycling: An optimal control study.**
637 *Journal of Applied Physiology* **134**, 980–991.
- 638 Lemaire, K. K., Baan, G. C., Jaspers, R. T. and Soest, A. J. van (2016). **Comparison of the validity of Hill
639 and Huxley muscle-tendon complex models using experimental data obtained from rat m. soleus in
640 situ**. *Journal of Experimental Biology* **219**, 2228.
- 641 Levin, A. and Wyman, J. (1927). **The viscous elastic properties of muscle**. *Proceedings of the Royal Society
642 of London. Series B - Biological Sciences* **101**, 218–243.
- 643 Petrofsky, J. S. and Phillips, C. A. (1981). **The influence of temperature, initial length and electrical
644 activity on the force-velocity relationship of the medial gastrocnemius muscle of the cat**. *Journal of
645 Biomechanics* **14**, 297–306.
- 646 Rack, P. M. H. and Westbury, D. R. (1969). **The effects of length and stimulus rate of tension in the
647 isometric cat soleus mouse**. *The Journal of Physiology* **204**, 443–460.
- 648 Reuvers, E. D. H. M., Maas, H., Noort, W., Bobbert, M. F. and Kistemaker, D. A. (2025). **Maximising
649 average mechanical power output during stretch-shortening cycles of rat medial gastrocnemius muscle.**
650 *bioRxiv*.
- 651 Rijkelijkhuijzen, J. M., De Ruiter, C. J., Huijing, P. A. and De Haan, A. (2003). **Force/velocity curves of
652 fast oxidative and fast glycolytic parts of rat medial gastrocnemius muscle vary for concentric but not
653 eccentric activity**. *Pflügers Archiv* **446**, 497–503.
- 654 Soest, A. J. van and Bobbert, M. F. (1993). **The contribution of muscle properties in the control of explosive**

- 655 movements. *Biological Cybernetics* **69**, 195–204.
- 656 **Soest, A. J. van, Gföhler, M. and Casius, L. J. R.** (2005). Consequences of ankle joint fixation on FES
657 cycling power output: A simulation study. *Medicine and Science in Sports and Exercise* **37**, 797–806.
- 658 **Stephenson, D. G. and Williams, D. A.** (1982). Effects of sarcomere length on the force—pCa relation in
659 fast- and slow-twitch skinned muscle fibres from the rat. *The Journal of Physiology* **333**, 637–653.
- 660 **Stern, J. T. Jr.** (1974). Computer modelling of gross muscle dynamics. *Journal of Biomechanics* **7**, 411–428.
- 661 **Walker, S. M. and Schrodт, G. R.** (1974). I segment lengths and thin filament periods in skeletal muscle
662 fibers of the rhesus monkey and the human. *The Anatomical Record* **178**, 63–81.
- 663 **Woittiez, R. D., Huijing, P. A., Boom, H. B. and Rozendaal, R. H.** (1984). A three-dimensional muscle
664 model A quantified relation between form and function of skeletal muscles. *Journal of Morphology* **182**,
665 95–113.
- 666 **Zajac, F. E.** (1989). Muscle and tendon: properties, models, scaling, and application to biomechanics and
667 motor control. *Critical Reviews in Biomedical Engineering* **17**, 359–411.
- 668 **Zandwijk, J. P. van, Bobbert, M. F., Baan, G. C. and Huijing, P. A.** (1996). From twitch to tetanus:
669 performance of excitation dynamics optimized for a twitch in predicting tetanic muscle forces .
670 *Biological Cybernetics* **75**, 409–417.
- 671 **Zandwijk, J. P. van, Baan, G. C., Bobbert, M. F. and Huijing, P. A.** (1997). Evaluation of a self-consistent
672 method for calculating muscle parameters from a set of isokinetic releases. *Biological Cybernetics* **77**,
673 277–281.

674 **Supplementary material**

675 **S1 Parameter value estimation toolbox**

676 The open-source toolbox automates muscle parameter estimation using data from quick-release, step-
677 ramp, and isometric experiments. Our associated manuscript demonstrates that accuracy improves when
678 correcting for CE shortening during quick-release. However, this requires both quick-release and step-
679 ramp data. Recognising that some users may only have one type of data, we designed the toolbox with
680 flexibility. The toolbox offers the following options:

681 **1. Estimate CE, SEE and PEE force-length parameters only**

- 682 • Requires *only* quick-release data.
- 683 • Does **not** correct for CE shortening due to the quick-release.

684 **2. Estimate CE force-velocity parameters only**

- 685 • Requires *only* step-ramp data.
- 686 • Since force-length parameter values are unknown, the following assumptions are made:
 - 687 a) CE velocity during ramp equals MTC velocity
 - 688 b) CE force equals SEE force
 - 689 c) CE length during ramp equals CE optimum length

690 **3. Estimate force-length and CE force-velocity parameters using the ‘traditional method’.**

- 691 • Requires *both* quick-release and step-ramp data.
- 692 • Does **not** correct for CE shortening due to the quick-release.

693 **4. Estimate force-length and CE force-velocity parameters using the ‘improved method’ (recommended)**

- 695 • Requires *both* quick-release and step-ramp data.
- 696 • **Does** correct for CE shortening due to the quick-release.

697 **5. Estimate (de-)activation dynamics parameters**

- 698 • Any data type may be used, but isometric contraction data is recommended to minimise the
699 influence of contraction dynamics (see manuscript).
- 700 • Can only be performed after estimating force-length and force-velocity parameters (via option
701 3 or 4).

702 The following sections explain how to use each option. Sample scripts are available for all options to further
703 assist with implementation.

704 **S1.1 CE, SEE and PEE force-length parameter value estimation**

705 First, extract the relevant data from the quick-release experiments by setting the configurations below:

```
optsQR = {
    'dataDir':      'C:/xxx/xxx/xxx/Data/QR/',
    'iCols':        (0,1,3),
    'idxQRmin':     [(0,20), (1,11), (60,85)],
    'idxQRpre':     'auto',
```

```
'idxQRpst':      'auto',
'nQRsamp':       'auto',
'dispFig':        True,
}
```

- 706 • **dataDir**: Path to your quick-release data files. If omitted, a file selector dialog will appear.
- 707 • **iCols**: Tuple indicating the columns representing 1) time; 2 MTC length and 3) SEE force, respectively.
708 If omitted, a column selector dialog will appear.
- 709 • **idxQRmin**: List of start and stop indices for the period with minimum SEE force. Provide ranges
710 for each quick-release experiment or use 'auto' for automatic detection.
- 711 • **idxQRpre**: List of start and stop indices for SEE force before the quick-release. Provide ranges for
712 each quick-release experiment or use 'auto' for automatic detection.
- 713 • **idxQRpst**: List of start and stop indices for SEE force after the quick-release. Provide ranges for
714 each quick-release experiment or use 'auto' for automatic detection.
- 715 • **nQRsamp**: Number of samples to average before and after the quick-release. Default is 5 if 'auto' or
716 unspecified.
- 717 • **dispFig**: When True, plots will be displayed for manual verification and adjustment of selected data
718 segments (i.e., idxQRmin, idxQRpre and idxQRpst).

719 Second, call the function 'loaddata.qr' to select the quick-release data:

```
dataQR, idxQRmin, idxQRpre, idxQRpst = loaddata.qr(optsQR)
```

- 720 • **dataQR**: List of dictionaries containing the extracted quick-release data.
- 721 • **idxQRmin**, **idxQRpre** and **idxQRpst**: Returned index ranges for your reference or future use.

722 Third, obtain the 'default' muscle parameter (such as width of the CE force-length relationship etc.):

```
defpar = loaddata.get_muspar()
```

- 723 • **defpar**: Dictionary containing the 'default' muscle parameter values.

724 Fourth, estimate the CE, PEE and SEE and force-length parameter values by passing your data and initial
725 parameters to 'estimate.fl':

```
estpar,dataQRout = estimate.fl(dataQR,defpar)
```

- 726 • **estpar**: Dictionary containing estimated muscle parameter values.
- 727 • **dataQRout**: List of dictionaries for each quick-release trial, with keys:
 - 728 – *lseeQRpre*: Estimated SEE length before quick-release
 - 729 – *lseeQRpst*: Estimated SEE length after quick-release
 - 730 – *fseeQRpre*: SEE force before quick-release
 - 731 – *fseeQRpst*: SEE force after quick-release
 - 732 – *lpeeQR*: (Estimated) PEE length of the data
 - 733 – *fpeeQR*: PEE force of the data

- 734 – *lmtcQRpre*: MTC length before quick-release

735 **S1.2 CE force-velocity parameter value estimation**

736 First, extract the relevant data from the step-ramp experiments by setting the configurations below:

```
optsSR = {  
    'dataDir': 'C:/xxx/xxx/xxx/Data/SR/ ',  
    'iCols': (0,1,3),  
    'idxSRcon': 'auto',  
    'nSRsamp': 10,  
    'dispFig': False,  
}
```

- 737 • **dataDir**: Path to your step-ramp data files. If omitted, a file selector dialog will appear.
738 • **iCols**: Tuple indicating the columns representing 1) time; 2) MTC length and 3) SEE force, respectively.
739 If omitted, a column selector dialog will appear.
740 • **idxSRcon**: List of start and stop indices where SEE force is most ‘constant’. If set to ‘auto’, indices are
741 automatically detected.
742 • **nSRsamp**: Number of data points to average during the constant force phase. Default is 10 if ‘auto’
743 or unspecified.
744 • **dispFig**: When True, plots will be displayed for manual verification and adjustment of selected data
745 segments (i.e., idxSRcon).

746 Second, call the function ‘*loaddata.sr*’ to select the step-ramp data:

```
dataSR, idxSRcon = loaddata.sr(optsSR)
```

- 747 • **dataSR**: List of dictionaries containing the extracted step-ramp data.
748 • **idxSRcon**: Returned index ranges for your reference or future use.

749 Third, obtain the ‘default’ muscle parameter (such as width of the CE force-length relationship etc.):

```
defpar = loaddata.get_muspar()
```

- 750 • **defpar**: Dictionary containing the ‘default’ muscle parameter values.

751 Fourth, estimate the CE force-velocity parameter values by passing your data and initial parameters to
752 ‘*estimate.fv*’:

```
estpar,dataSRout = estimate.fv(dataSR,defpar)
```

- 753 • **estpar**: Dictionary containing the estimated muscle parameters.
754 – If only CE force-velocity parameters are estimated (option 2), a , b , and F_{CE}^{max} are estimated on
755 based step-ramp data.
756 – If combined with estimation of force-length parameters (option 3 & 4), a , b are estimated on
757 based step-ramp data (while F_{CE}^{max} is estimated based on quick-release data).

- 758 • **dataQRout:** List of dictionaries for each quick-release trial, with keys:
759 – *vceSR*: Estimated CE shortening velocity.
760 – *fceSR*: Estimated CE force.
761 – *lcerelSR*: Relative CE length.

762 **S1.3 Traditional method**

763 Running the traditional method requires first estimating the CE, SEE and PEE force-length parameter
764 values and then CE force-velocity parameter values. All inputs and outputs of the function are described
765 above.

```
#%% Get default muscle parameters
defpar = loaddata.get_muspar()

# %% Settings and load data
optsQR = {
    # Include your options here
}
optsSR = {
    #Include your options here
}
dataQR, idxQRmin, idxQRpre, idxQRpst = loaddata.qr(optsQR)
dataSR, idxSRcon = loaddata.sr(optsSR)

# %% Run uncorrected method
estpar, dataQRout = estimate.fl(dataQR, defpar)
estpar, dataSRout = estimate.fv(dataSR, defpar, estpar)
```

766 **S1.4 Improved method**

767 To run the improved method, call a separate function ‘estimate.im’. This function iteratively call ‘estimate.fl’
768 and ‘estimate.fv’ until the change in all estimated parameter values are below 0.1%. All inputs and outputs
769 of the function are described above.

```
#%% Get default muscle parameters
defpar = loaddata.get_muspar()

# %% Settings and load data
optsQR = {
    # Include your options here
}
optsSR = {
    #Include your options here
}
```

```
    }

dataQR, idxQRmin, idxQRpre, idxQRpst = loaddata.qr(optsQR)
dataSR, idxSRcon = loaddata.sr(optsSR)

# %% Run improved method
estpar, dataQRout, dataSRout = estimate.im(dataQR, dataSR, defpar)
```

770 **S1.5 Excitation dynamics parameter value estimation**

771 To estimate the time constants of the calcium dynamics, one has to first estimate the parameter values of the
772 CE, PEE and SEE force-length relationships as well as the parameters of the CE force-velocity relationship.
773 After this the time constant of the calcium dynamics can be estimated. First, extract the relevant data
774 (from the quick-release experiments) by setting the configurations below:

```
optsISOM = {
    'dataDir': dataDir+'ISOM',
    'iCols': (0,1,3,2),
    'durStimOffset': 0.1,
    'dispFig': False,
}
```

- 775 • **dataDir**: Path to your (isometric) data files. If omitted, a file selector dialog will appear.
776 • **iCols**: Tuple indicating the columns representing 1) time; 2 MTC length and 3) SEE force, respectively.
777 If omitted, a column selector dialog will appear.
778 • **durStimOffset**: Time (in seconds) to include after stimulation offset. If not specified, the default is
779 0.1 s.
780 • **dispFig**: When True, plots will be displayed for manual verification of selected data segments (i.e.,
781 idxSRcon).

782 Second, call the function ‘SelISOMdata’ to select the (isometric) data:

```
dataISOM, idxSEL = SelISOMdata(optsISOM)
```

- 783 • **dataISOM**: List of dictionaries containing the extracted (isometric) data.
784 • **idxSEL**: List of start and stop indices of selected interval of the data.
785 Third, estimate the excitation dynamics parameter values by passing your data and initial parameters to
786 ‘getACTparms’:

```
estpar, dataACTout = estimate.act(dataISOM, defpar, estpar)
```

- 787 • **estpar**: Dictionary containing the estimated muscle parameters.
788 • **dataACTout**: List of dictionaries for each (isometric) experiment, with keys::
789 – *time*: Time-axis.
790 – *lmtc*: MTC length.

- 791 – *fseeData*: Experimental SEE force.
792 – *fseeMdl*: Model-predicted SEE force.
793 – *tStim*: List containing stimulation onset and offset times.

794 **S2 Supplemental Figures**

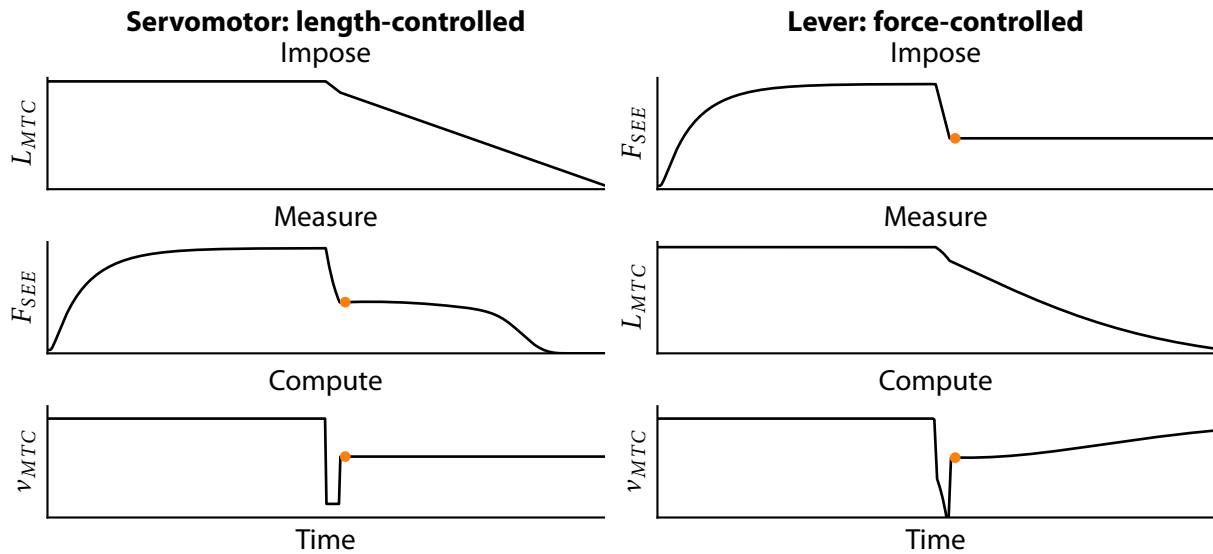


Figure S1: Comparison between a length-controlled step-ramp experiment and a force-controlled quick-release experiment. In length-controlled step-ramp experiment (left), MTC length over time is imposed using a servomotor, while SEE force is measured. MTC velocity is computed at the time instance at which SEE force is near constant. In the force-controlled quick-release experiment (right), SEE force over time is imposed via a lever, while MTC length is measured. MTC velocity is computed at the time instance where MTC velocity is maximal after the change in SEE force. Both methods yield one datapoint (depicted with the orange dot) of the force-velocity relationship.

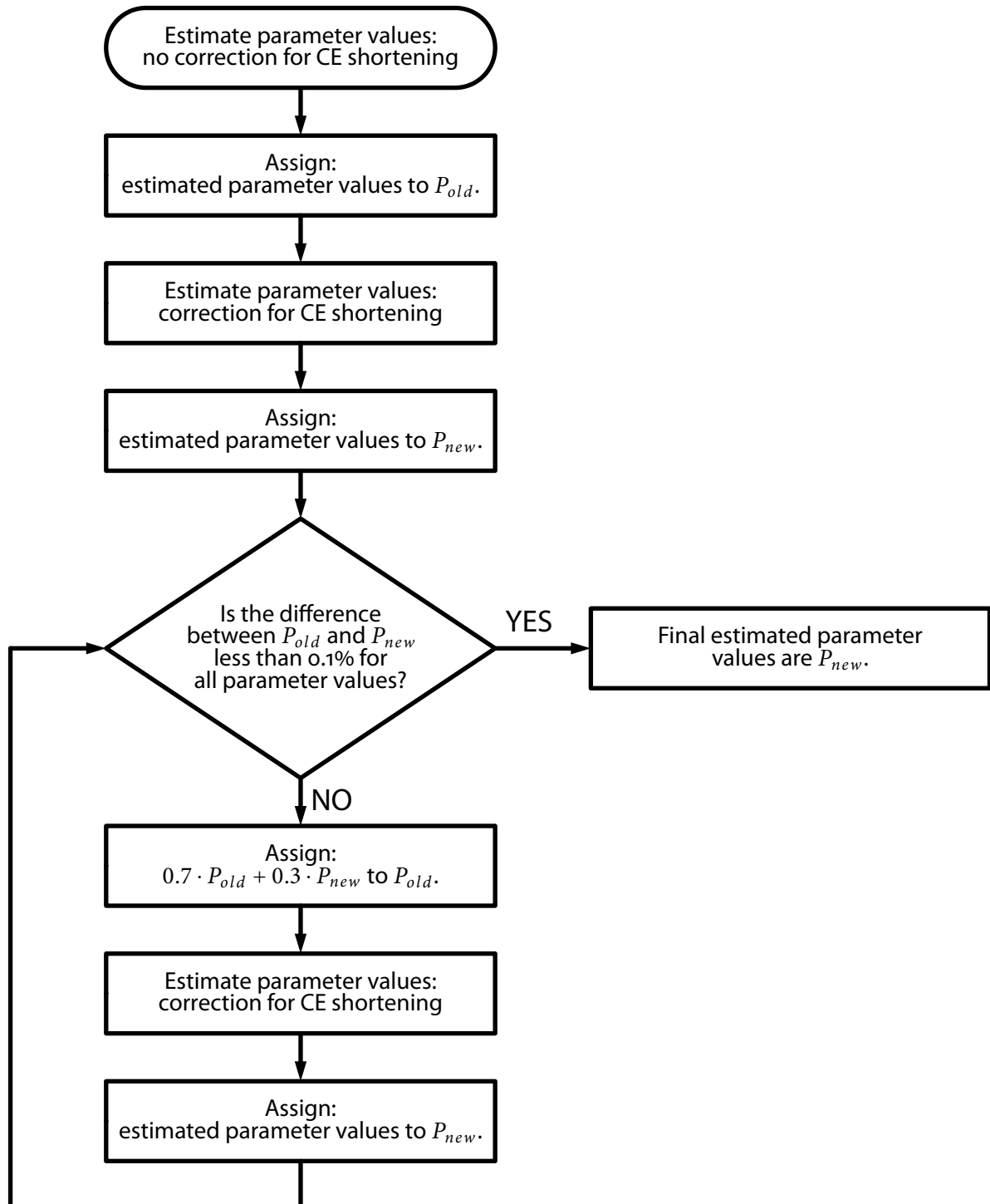


Figure S2: Flowchart of the improved method. Using the improved method, parameter values were estimated until the change in all parameter values was less than 0.1%.

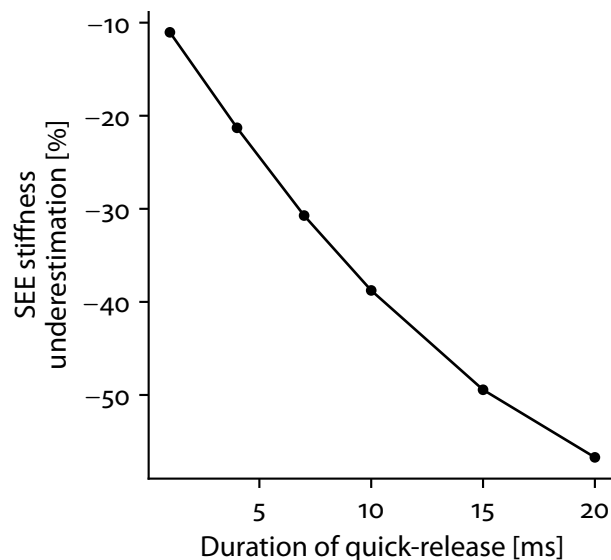


Figure S3: Relationship between quick-release duration and SEE stiffness underestimation. When the duration of the quick-release increases, the underestimation of SEE stiffness increases.

795 **S3 Supplemental Tables**

Table S1: MTC parameter values obtained from literature to simulate data.

| Parameter | Unit | GM1 | GM2 | GM3 | Reference |
|-----------------------------|-------------------|----------------------|----------------------|----------------------|--|
| <i>Contraction dynamics</i> | | | | | |
| a | N | 2.68 | 1.80 | 2.58 | van Zandwijk et al. (1996) |
| b | mm | 41.6 | 24.8 | 41.8 | van Zandwijk et al. (1996) |
| b_{scale}^{min} | - | | 0.100 | | van Soest and Bobbert (1993) |
| b_{shape} | - | | 22.0 | | van Soest and Bobbert (1993) |
| F_{asym} | - | | 1.50 | | Rijkelhuizen et al. (2003) |
| F_{CE}^{max} | N | 13.4 | 13.8 | 12.3 | van Zandwijk et al. (1996) |
| k_{PEE} | N/mm ² | 213 | 165 | 511 | van Zandwijk et al. (1996) |
| k_{SEE} | N/mm ² | 4220 | 3640 | 3470 | van Zandwijk et al. (1996) |
| L_{CE}^{opt} | mm | 13.2 | 12.3 | 11.2 | van Zandwijk et al. (1996) |
| L_{PEE}^o | mm | 13.9 | 13.2 | 13.4 | van Zandwijk et al. (1996) |
| L_{SEE}^o | mm | 28.3 | 30.3 | 26.5 | van Zandwijk et al. (1996) |
| r_{as} | - | $3.71 \cdot 10^{-3}$ | $5.45 \cdot 10^{-3}$ | $3.16 \cdot 10^{-3}$ | Arbitrary small value |
| <i>Excitation dynamics</i> | | | | | |
| r_{slope} | mm | | 2.00 | | Katz (1939) |
| w | - | | 0.50 | | Burkholder and Lieber (2001) |
| a_{act} | - | | -7.37 | | Bortolotto et al. (2000) |
| $b_{act,1}$ | - | | 5.17 | | Bortolotto et al. (2000) |
| $b_{act,2}$ | - | | 0.596 | | Stephenson and Williams (1982) |
| $b_{act,3}$ | - | | 0.00 | | Stephenson and Williams (1982) |
| kCa | mol/L | | $8.00 \cdot 10^{-6}$ | | Kistemaker et al. (2005) |
| γ_o | - | | $1.00 \cdot 10^{-5}$ | | Arbitrary small value |
| q_o | - | | $5.00 \cdot 10^{-3}$ | | Hatze (1981) |
| τ_{act} | ms | | 27.0 | | van Zandwijk et al. (1996) |
| τ_{deact} | ms | | 27.0 | | van Zandwijk et al. (1996) |

Table S2: Estimated parameter values of the experimentally measured *in situ* data using both the traditional as well as the improved method.

| Parameter | Unit | <i>Traditional method</i> | | | <i>Improved method</i> | | |
|------------------|-------------------|---------------------------|--------------|--------------|------------------------|--------------|--------------|
| | | Rat 1 | Rat 2 | Rat 3 | Rat 1 | Rat 2 | Rat 3 |
| <i>a</i> | N | 8.90 | 11.3 | 10.5 | 8.82 | 10.0 | 11.0 |
| <i>b</i> | mm | 76.7 | 108 | 84.6 | 81.9 | 105 | 90.6 |
| F_{CE}^{max} | N | 15.6 | 14.1 | 17.1 | 15.5 | 14.1 | 17.0 |
| k_{PEE} | N/mm ² | 9.83 | 7.25 | 21.9 | 28.7 | 24.1 | 34.8 |
| k_{SEE} | N/mm ² | 608 | 688 | 654 | 952 | 1260 | 1050 |
| L_{CE}^{opt} | mm | 12.4 | 12.9 | 12.3 | 13.7 | 14.7 | 13.3 |
| L_{PEE}^o | mm | 12.4 | 12.4 | 13.3 | 15.1 | 15.6 | 14.5 |
| L_{SEE}^o | mm | 29.0 | 29.7 | 25.1 | 28.8 | 29.3 | 25.2 |
| τ_{act} | ms | 43.0 | 32.4 | 23.6 | 55.2 | 57.7 | 41.6 |
| τ_{deact} | ms | 23.8 | 20.9 | 19.7 | 27.1 | 25.3 | 22.4 |

Table S3: Root mean squared differences between experimentally measured SEE force histories and those predicted by Hill-type MTC model after estimating all contraction and excitation dynamics parameter values.

| | <i>Traditional method</i> | | | | <i>Improved method</i> | | | |
|---------------|---------------------------|---------------|---------------|---------------|------------------------|---------------|---------------|---------------|
| | QR | SR | ISOM | SSC | QR | SR | ISOM | SSC |
| Rat 1 | 5.6 ± 3.4 | 5.6 ± 0.8 | 6.8 ± 3.2 | 6.2 ± 3.0 | 3.3 ± 1.5 | 2.8 ± 0.9 | 5.4 ± 3.0 | 5.4 ± 3.1 |
| Rat 2 | 4.2 ± 1.5 | 5.0 ± 0.6 | 4.3 ± 1.6 | 4.6 ± 2.2 | 2.7 ± 1.6 | 2.1 ± 0.5 | 4.2 ± 2.6 | 4.2 ± 2.0 |
| Rat 3 | 6.4 ± 2.3 | 6.8 ± 1.0 | 6.1 ± 2.1 | 5.5 ± 2.7 | 4.2 ± 1.8 | 2.6 ± 0.5 | 4.9 ± 2.3 | 5.0 ± 2.7 |
| Avg \pm Std | 5.4 ± 2.6 | 5.8 ± 1.1 | 5.7 ± 2.7 | 5.4 ± 2.7 | 3.4 ± 1.8 | 2.5 ± 0.7 | 4.8 ± 2.7 | 4.9 ± 2.7 |

Root mean squared differences are expressed as a percentage of the maximal isometric CE force (F_{CE}^{max}). Root mean squared differences were computed over the interval in which CE stimulation was maximal for the quick-release and step-ramp experiments and was computed over the interval from CE stimulation onset to 0.1 s after CE stimulation ceased for the isometric experiments and the stretch-shortening cycles.